SEP 18 1958
13904
Copy 239
RM L58G03

[redacted]L

NACA RM L58G03

TECH LIBRARY KAFB, NM
0144755

7847

NACA

RESEARCH MEMORANDUM

Classification cancelled (or changed to .....)
By Authority of ..... (OFFICER AUTHORIZED TO CHANGE)
By ..... (NAME AND GRADE OF OFFICER MAKING CHANGE)
DATE

FREE-FLIGHT INVESTIGATION OF AERODYNAMIC HEAT TRANSFER TO A SIMULATED GLIDE-ROCKET SHAPE AT MACH NUMBERS UP TO 10

By Andrew G. Swanson

Langley Aeronautical Laboratory
Langley Field, Va.

CLASSIFIED DOCUMENT

This material contains information affecting the National Defense of the United States within the meaning of the espionage laws, Title 18, U.S.C., Secs. 793 and 794, the transmission or revelation of which in any manner to unauthorized person is prohibited by law.

NATIONAL ADVISORY COMMITTEE
FOR AERONAUTICS

WASHINGTON
September 10, 1958

CONFIDENTIAL

AFMDC DAS '58-6871

TECH LIBRARY KAFB, NM
0144755

NATIONAL ADVISORY COMMITTEE FOR AERONAUTICS

RESEARCH MEMORANDUM

FREE-FLIGHT INVESTIGATION OF AERODYNAMIC HEAT TRANSFER TO A SIMULATED GLIDE-ROCKET SHAPE AT MACH NUMBERS UP TO 10*

By Andrew G. Swanson

SUMMARY

Heat-transfer measurements were made on a simulated glide-rocket shape in free flight at Mach numbers up to 10 and free-stream Reynolds numbers of 2×10^6 based on distance along surface from apex and 3×10^4 based on nominal leading-edge diameter. The model simulated the bottom of a 75° delta wing at 8° angle of attack. The data indicated that for the test conditions a modified three-dimensional stagnation-point theory will predict to reasonable engineering accuracy the heating on a highly swept wing leading edge, the heating being reduced by sweep by the 3/2 power of the cosine of the sweep angle. The data also indicate that laminar heating rates over the windward surface of a highly swept flat glider wing at moderate angles of attack can be predicted with reasonable engineering accuracy by flat-plate theory using wedge local flow conditions and basing Reynolds numbers on lengths from the wing leading edge parallel to the surface center line.

INTRODUCTION

In view of the current interest in glide rockets, a free-flight investigation of aerodynamic heat-transfer characteristics of a glide-rocket shape has been made. The model configuration simulated a flat-bottomed delta wing having a blunt leading edge swept approximately 75° and flying at a trim angle of attack of 8°. In order to obtain a symmetrical shape for flight test, the wing was simulated by a three-sided pyramidal shape, each surface of which would have heating characteristics similar to the undersurface of the glide missile; the edges of the pyramid would approximately simulate the leading edges of the glide missile wing. The test shape was tested with the same five-stage research missile system used in the investigations reported in references 1 to 4.

Although the model reached a maximum Mach number of 14.7 at an altitude of 88,100 feet, the stability of the fifth stage seemed to be

*Title, Unclassified.

AFMDC DAS '58-6871

marginal and the model flew at a large and somewhat indeterminant angle of attack; thus, temperature data obtained during this portion of the flight are difficult to analyze. However, during the fourth-stage burning, heat-transfer data were obtained at Mach numbers up to 10 and free-stream Reynolds numbers of about 2×10^6 based on the rearmost thermocouple location on the flat surface and 0.3×10^5 based on leading-edge diameter.

The fourth-stage rocket motor (JATO, 1.52-KS-33550, XM-19 (Recruit)) used in the present investigation was made available by the U. S. Air Force.

SYMBOLS

A	cross-sectional area at reference station, sq ft
A_N	normal acceleration, gravitational units
A_T	transverse acceleration, gravitational units
C_{L_α}	lift-curve slope per degree
h	enthalpy, Btu/slug
k	thermal conductivity, Btu/ft-sec-$^\circ$R
l	distance between thermocouples, ft
M	free-stream Mach number
q	heating rate, Btu/sec-ft^2
q_d	dynamic pressure, lb/sq ft
R_∞	Reynolds number based on free-stream conditions
R_D	Reynolds number based on free-stream conditions and twice leading-edge radius
S	surface area used in conduction corrections, sq ft
t	time, sec
T	temperature, $^\circ$R unless otherwise noted

W	weight, lb
x	distance, ft
$\frac{dU}{dx}$	velocity gradient, 1/sec
α	angle of attack, deg
θ	orientation of resultant acceleration vector, deg
Λ	sweep angle, deg
μ	viscosity, slugs/ft-sec
ρ	density, slugs/cu ft

Subscripts:

theo	theory
w	wall
s	stagnation
3D	three-dimensional
aw	adiabatic wall
∞	free stream
res	resultant
n	thermocouple number

MODEL AND TEST

Model Configuration

The fifth stage of the missile system used in this investigation consisted of a three-sided pyramidal test nose which had a blunted apex, a stepped cylindrical midsection, and a 20° total angle conical frustum tail. A photograph of the fifth stage is shown in figure 1; pertinent dimensions are given in the sketch (fig. 2) which also shows dimensions of the forth- and fifth-stage combination. The test nose simulated a

AFMDC DAS '58-6871

glide rocket shape, and nose details are shown in the sketch of figure 3 and the photographs of figure 4.

The test nose was fabricated from Inconel of 0.05-inch nominal thickness. One edge of the pyramid was rolled to an exterior radius of 0.10 inch, and the resulting two surfaces were welded at the edges to a third surface. The pyramid thus formed was welded to an Inconel cylinder at the lines of intersection of the pyramid and cylinder. The forward end of the nose was formed from a block of nickel.

A conical radiation shield was mounted inside the test nose and bolted to the nickel block at the forward end. The after end of the test nose was slip-fitted over a micarta block attached to the radiation shield. The thermocouple switching motor was attached to a bracket within the radiation shield.

A double-walled Inconel cylindrical section behind the nose housed most of the telemetering equipment. The stepped conical section contained an alumina insulating ring, which was used to isolate electrically the two ends of the fifth stage to form the telemeter antenna. The Fiberglas lined, Inconel conical frustum at the after end was intended to give the fifth stage static stability and also to serve as an extension to the rocket-motor nozzle.

The pyramidal nose was polished to a general surface roughness of 10 microinches or less as determined optically by a fringe-interferometer microscope. There were, however, several pits and scratches which were considerably deeper than the 10-microinch level; these did not seem to have significant effects on the data measured.

Instrumentation

Measurements of the output of 24 thermocouples and 4 accelerometers were transmitted from the test vehicle during flight by a six-channel telemeter. The chromel-alumel thermocouples were made from No. 30 gage wire and were spot welded to the inner surface of the skin of the test nose. The two leads of each thermocouple were welded separately to the skin with a spacing between the leads of about 1/32 inch to 1/16 inch. Those thermocouples located behind the leading-edge stagnation line had the spacing lengthwise along the leading edge; that is, both thermocouple leads were on a line parallel to the stagnation line. The thermocouple located in the nickel block at the forward stagnation point was welded at the bottom of a tapped hole and the leads were led through the hollow bolt which supported the radiation shield. The locations of the thermocouples are shown in figure 5. Wall thicknesses measured at the various thermocouple stations are given in table I.

Three constant voltages and outputs of 12 thermocouples were commutated by a switching motor and transmitted by one telemeter channel at a sampling rate of about 6 per second; the remaining 12 thermocouples and the 3 constant voltages were transmitted in similar fashion on another telemeter channel. The constant voltages served as in-flight references for calibration of the thermocouple-telemeter system. The voltages were chosen to be equivalent to the low end, middle, and high end of the range for which the thermocouples were calibrated. Since the range was chosen on the basis of possible turbulent heat transfer and since the flow was primarily laminar during the test, the actual measured temperatures were less than one-half of the full-scale range.

Each of the four remaining telemeter channels was used to transmit a continuous measurement of the output of an accelerometer; two of these measured longitudinal accelerations, one measured normal accelerations, and one transverse accelerations. The accelerometers were calibrated in standard earth gravitational units g for the following ranges:

Longitudinal accelerometers . . . . . -50g (drag) to 150g (thrust)
Normal and transverse
accelerometers . . . . . -25g to 25g

Other instrumentation consisted of ground-based radars for measuring velocity during the early portion of the flight and for determining space position of the missile system. A radar-tracked radiosonde balloon was used to determine atmospheric conditions and wind velocity; these data were determined at the altitude of the high-speed portion of the flight within about one-half hour of the flight.

Flight

The propulsion system consisted of five stages of solid fuel rocket motors. The test nose, which was attached to the fifth stage, and the booster stages are shown on the launcher in figures 6 and 7. Characteristics of the rocket motors and stage weights for a similar five-stage system are tabulated in reference 3; these data are also applicable to the test reported herein.

The missile system was launched at an elevation angle of 73°. The first two stages were used to propel the remaining three stages to a peak altitude of about 94,200 feet. Just after apogee, when the flight path was inclined downward at about 2°, a preset mechanical timer fired the third stage. Shortly after third-stage burnout, a delay squib, ignited at third-stage ignition, fired the fourth stage; firing of the fifth stage was accomplished by use of a pressure switch, mounted on the fourth stage, which closed when the chamber pressure decreased as the fourth-stage motor burned out.

DATA REDUCTION

Trajectory Data

Velocity of the missile system for the first 28 seconds of flight was obtained from the ground-based Doppler radar. Thereafter, velocity was obtained from differentiation of the space-position radar data until third-stage ignition; from then until fifth-stage burnout, velocity data were obtained from integration of the longitudinal accelerometer data. The flight path was determined from the space-position radar data from launching time until third-stage ignition; shortly after this time the radar ceased to track the missile system. The flight path was then reconstructed by double integration of the longitudinal accelerometer data.

Heat-Transfer Data

The aerodynamic heat transfer to the model was obtained from the thermocouple data which gave temperature time histories for the inside surface of the skin of the test nose. These temperature data are normally reduced by use of the reference calibration voltage measured after each sampling cycle of the thermocouple. In this test, shifts were noted in the reference voltages at the times of rocket-motor firing and small, slow, but persistent drifts at other times. Consequently, the thermocouple data were reduced by use of calibration voltages recorded both before and after each sampling cycle of the thermocouple outputs. These points were plotted and a curve drawn through the average of, or the most consistent of, the data points obtained at each time.

These faired inside-surface temperature curves, together with the one-dimensional heat-flow-analysis method of reference 5 for thermally thick walls, were used to compute outside wall temperatures. This computing method exhibits tendencies toward instability when small time intervals are used if the time rate of increase of inside wall temperature is small. In order to obtain more points at a larger time interval, two separate computations of outside temperature were made at intervals half as large and then the two were joined together to give the outside temperature history. The analysis assumes constant thermal properties for the wall, and the values used were those for a temperature midway between the highest and lowest measured temperatures for each station; this use of constant thermal properties is believed to introduce small error in the final heat-transfer data. In general, the computed outside wall temperatures were used directly in the one-dimensional analysis method of reference 5 to determine the aerodynamic heat input to the skin of the test nose, again on the assumption of constant wall thermal properties.

For the thermocouples on the leading edge, the actual physical thickness of the skin was not used in computing temperature and heating rates. Since the heat flow into the outer surface tends to be "focused" toward the center of the leading-edge radius, an effective leading-edge thickness equal to the ratio of the leading-edge volume to the external surface area was used. For the geometry of the configuration tested, the effective thickness was about three-quarters of the actual thickness. The heating rates computed with this effective thickness were about 10 percent to 30 percent less than the rates computed with the actual leading-edge thickness.

Corrections for Conduction

Conduction effects in the longitudinal direction (or along any ray from the apex) on the test nose were estimated to be negligible. Conduction effects in the lateral direction (or across the nose) were also estimated to be negligible except near the corner or leading edge. Lateral conduction corrections were approximated by a method similar to that of reference 3. A lateral strip of unit width on the nose was divided into blocks approximately centered about a thermocouple. The change in heat flow at a station n is then given by

$$\Delta q_n = \frac{kA_{n+1}}{S_n} \frac{T_n - T_{n+1}}{l_{n+1}} + \frac{kA_{n-1}}{S_n} \frac{T_n - T_{n-1}}{l_{n-1}}$$

At the corner, the block surface area S_n was taken as the area between points where the leading-edge circumference became tangent to the flat surfaces; the remaining block edges were then taken at stations midway between thermocouples. The areas A_n are, of course, the cross-sectional area of the skin; lengths between thermocouples l_n were taken at a distance two-thirds of the way out from the inside surface. Outside surface temperatures were used in these calculations.

This method of correcting for lateral heat flow is not exact; it assumes, for example, that the heat flows through and along the skin can be calculated independently and the resulting solutions superimposed. It is believed that insufficient temperature-distribution data were obtained to warrant a more rigorous analysis. The general conclusions regarding the overall heat transfer would not, however, be likely to be modified by even fairly large changes in the estimate of these lateral heat flow corrections.

Radiation heat losses were estimated to be negligible and were therefore not included in the analysis.

ACCURACY

Trajectory Data

The possible inaccuracies in the Mach number at the time of third-stage ignition are estimated to be less than ±0.1. Integration of the accelerometers for velocity after this time gives an accumulative error with time. This would result in an additional possible error in the Mach number at fifth-stage burnout which is estimated to be less than ±0.5. In view of the consistency between preflight trajectory estimates and the flight test results for velocity increments for each stage of the flight for this test and the tests reported in references 1 to 4 (for which similar propulsion systems were used), the Mach numbers are believed to be more accurate than the foregoing figures would indicate.

Uncertainties in the flight-path angle due to failure of the space-position radar to track the test vehicle after third-stage ignition result in estimated possible inaccuracies in altitude at fifth-stage burnout of less than ±2,000 feet.

Temperature and Heat-Transfer Data

The full-scale temperature range (chosen on the basis of possible turbulent flow at $M = 15$) was 1700° F, which results in an estimated possible basic temperature data inaccuracy of ±17° F. The level of the curve faired through the measured data points has an estimated possible error of about ±5° F. Since the heating rates were fairly low during the primary-data-measurement period (fourth-stage burning) possible inaccuracies computed for the final heat-transfer data would be fairly large. However, in view of the reasonable consistency of most of the data, the accuracy is believed sufficient to warrant the conclusions drawn. A more quantitative picture of the accuracy of the heat-transfer data is presented in the "Results and Discussion" section.

RESULTS AND DISCUSSION

Flight Path

Flight-test data were obtained as the test vehicle moved along the trajectory shown in figure 8. Times of significant events are indicated on the trajectory. Atmospheric conditions determined from the radiosonde data are shown in figure 9 as functions of time from third-stage ignition until fifth-stage burnout. Altitude and velocity data are shown in figure 10 for the same time interval. The telemeter signal from the test

vehicle failed momentarily just before fifth-stage burnout and ceased abruptly just as the fifth stage began to decelerate after burnout; evidently the test vehicle failed structurally at this time.

Test-Vehicle Stability

Plotted in figure 11 are the magnitudes of the normal and transverse accelerations measured by the accelerometers, and in figure 12 are the angles of attack estimated from these accelerations. The accelerations and estimated angle of attack were of negligible magnitude up to the time of fourth-stage ignition. The fourth- and fifth-stage combination evidently received a disturbing force as it separated from the third stage. This disturbance was fairly well damped near the time of fourth-stage burnout.

At fifth-stage ignition ($t = 89.5$ sec), the test vehicle started a somewhat divergent motion; the motion was not, however, purely divergent, as is shown by the oscillatory nature of the acceleration data (fig. 11). The exact reason for this apparent instability is not known; probably there was insufficient static stability, although it is possible that the vehicle was damaged at separation from the fourth stage. The test vehicle was originally developed for tests of blunt noses; the calculated stability for the sharper (and higher lift) nose of the present test was less than for the blunter nose models, although still presumably adequate. Probably the stabilizing force of the flare was overestimated and the use of the sharper nose changed the amount of stability from just adequate to rather marginal. Note that tests of the blunt-nose configurations of references 1, 3, and 4 showed small or negligible angle of attack while the test of a sharper nose of reference 2 showed significant angle of attack (although less than the angles apparently reached by the test vehicle of this test).

As is shown in the angle-of-attack data (fig. 12), there was a tendency for the fifth stage to trim at angle of attack; the steadily decreasing weight as the propellant burned would result in the measured increasing normal acceleration for a constant trim angle. There was undoubtedly some rolling motion; however, polar plots of the resultant acceleration vector established no consistent trend to a rolling motion, and it is believed that the motion was mainly purely oscillatory in the pitch and yaw planes.

From the resultant acceleration vector, resultant angles of attack were computed from the equation

$$\alpha_{res} = \frac{W\sqrt{A_N^2 + A_T^2}}{C_{L_\alpha} q_d A}$$

where linear weight variations with time were assumed during rocket-motor burning. Since force data were not available for the configuration tested, estimates of zero-lift C_{L_α} were used, 0.12 per degree based on a 9-inch-diameter body area for the fourth- and fifth-stage combination and 0.07 per degree based on the 6.2-inch-diameter body cross-section area for the fifth stage. This probably gives an overestimate of the actual model angle at the higher angles of attack, since the lift-curve slope would be expected to be nonlinear and to increase with angle of attack.

The angles of attack plotted in figure 12 are the angles determined from the resultant acceleration vectors and are average angles faired through the oscillations. Also plotted in figure 12 are the orientations of the resultant acceleration vector. The motion can be seen to be one primarily in the pitch plane. Note that only in the time from about 88.4 to 89.5 seconds (the latter part of fourth-stage burning) are the estimated angles of pitch and yaw small (1° or 2° or less). Contributing to the large angle of attack occurring at fourth-stage ignition is the relatively low dynamic pressure at this time (about 500 pounds per square foot); this dynamic pressure steadily increased to about 2,700 pounds per square foot at fourth-stage burnout and about 6,200 pounds per square foot at fifth-stage burnout.

The approximate angles of attack calculated are referred to in the rest of the discussion as estimated angles; the limitations in accuracy discussed above are implied.

Basic Temperature Data

The values of inside surface temperatures determined from the telemeter records are shown for several typical stations in figure 13 for times from 87 seconds on. The data before $t = 87$ seconds had similar scatter. Shown in figure 13(a) are data for thermocouples 2 and 16 (located on the leading-edge stagnation line) and in figure 13(b) are data for thermocouples 4 and 21 (located on the center line of the flat surface which contained most of the thermocouples). The lower set of curves on each of these figures was obtained from one thermocouple channel; the upper set of curves was obtained from the other thermocouple channel. Faired through the data points (which are shown as reduced from calibrate voltages before and after each sampling cycle as mentioned in the data reduction section) are the curves used for computation of outside surface temperature. Shown in figure 13(c) are the data points and faired inside surface temperature for thermocouple 1, which was located behind the nose stagnation point, along with a computed outside wall temperature variation. Thermocouple 1 was installed to give a qualitative indication of possible nose-tip melting; uncertainties as to

conduction corrections and directions of heat flow into this thermocouple precluded any analysis of heat transfer at this station. It is apparent, however, that high heating rates existed at the stagnation point and that at about the time of fifth-stage burnout, the forward stagnation surface was beginning to melt; this melting may have contributed to the model failure which evidently occurred as the test vehicle began to decelerate. The temperatures were of the order of those that would be expected for the flat-faced nose stagnation point.

Inside temperatures read from the curves faired through the measured data points are tabulated for all thermocouples and for several times during the flight in table II.

Computed Outside Wall Temperatures and Heating Rates

Shown in figure 14 are typical time histories of computed outside wall temperatures. The data are presented for the time periods during which the angle of attack was sufficiently small and the heating rates sufficiently high to provide reasonable heat-transfer data. Shown are the faired inside temperatures, the computed outside temperature points, and the curve faired through these computed points. The outside temperatures computed could generally be used directly in the computation of heat-transfer rates; however, stable oscillations arising in the numerical analysis occasionally necessitated fairing. The heating rates were in some cases sufficiently high for significant temperature gradients through the skin to exist.

The computed heating rates to the outside surface (one-dimensional heat flow through skin with lateral conduction neglected) are shown for several typical stations in figure 15. Both computed points and the curve faired through them are shown. When the actual aerodynamic heating rates are low, slopes of the measured temperature time histories, which are proportional to heating rate, are, of course, also low. At these times inaccuracies in temperature slope determination result in fairly large amounts of scatter in the heat-transfer data.

Also shown in figure 15 are typical data including conduction corrections. The corrections are by no means negligible for stations on or near the leading edge; however, fairly large percentage changes in the conduction corrections would be required to alter the basic conclusions drawn from the data.

An idea of the possible quantitative accuracy of the final heat-transfer data is probably best determined from the scatter of the data of figure 15.

Theory Used for Leading-Edge Heat Transfer

The theory used for comparison with the experimental leading-edge heat transfer was a modification of the Fay and Riddell theory (ref. 6) for three-dimensional stagnation-point heating. This theory was used mainly because of its ease of calculation (when appropriate simplifications are used). The basic theory of reference 6 is

$$q_{theo_{3D}} = 0.94(\rho_w\mu_w)^{0.1}(\rho_s\mu_s)^{0.4}(h_s - h_w)\left(\frac{dU}{dx}\right)_{s,3D}^{1/2}$$

for a Prandtl number of 0.71 and a Lewis number of 1.0. Reference 7 shows that, for the conditions of this test, varying Lewis number between 1 and 2 has small effect on the heating rate. The above expression is quite easily evaluated if the Sutherland variation of viscosity with temperature is used (ref. 6 indicates this law to be reasonably valid for temperatures up to 9000° K) and if ideal gas relations are used. The use of ideal-gas rather than real-gas relations should result in negligible differences in heating rates for the conditions of this test (as indicated in ref. 1) except possibly for the effect in $\left(\frac{dU}{dx}\right)_{s,3D}$. This parameter was evaluated from the theory of Korobkin for Mach numbers up to 5 and from Newtonian flow pressure distributions for higher Mach numbers. (See curve in fig. 16 of ref. 1.) The use of real-gas rather than perfect-gas relations for $\left(\frac{dU}{dx}\right)_s$ would lower the theoretical heating rates by about 5 to 10 percent at $M = 10$ and by lesser amounts at lower Mach numbers. It can be argued that for application of the theory to the swept leading edge, the real-gas effects on $\left(\frac{dU}{dx}\right)_s$ should be applied on the basis of Mach number normal to the leading-edge shock rather than free-stream Mach number; for the conditions of this test, there would then be negligible real-gas effects on $\left(\frac{dU}{dx}\right)_s$.

Two additional factors were necessary to convert this three-dimensional heating rate to a rate for a swept leading edge. First, the three-dimensional rates were converted to a two-dimensional rate by multiplying by the factor $\frac{1}{\sqrt{2}}$, which was used by Lees (ref. 8) and was shown to be approximately correct by Reshotko and Cohen (ref. 9). For the ratio $\frac{T_w}{T_s}$ for this test, reference 9 would indicate that this factor might be more appropriately 0.72 to 0.73 instead of 0.707. Second, this heating rate at the stagnation point of an unswept cylinder

must be modified to account for the reduction in heating rates due to sweep. For the results given herein, the factor used was $(\cos \Lambda)^{3/2}$; the validity of this factor (which has some theoretical justification) is discussed subsequently.

Experimental Leading-Edge Heat Transfer

The experimental heating rates on the leading (or pyramid) edge are shown in figure 16 as ratios with respect to theoretical heating rates for several times (and Mach numbers) during the flight. Data are presented for times near the end of third-stage burning when the measured rates were somewhat greater than the scatter in the data and for times during fourth-stage burning when the estimated angle of attack was reasonably low.

The experimental data, in general, are in agreement with or are less than the values predicted by the theory given in the previous section. The data for 86 seconds and 87 seconds were obtained during third-stage burning when there was marked scatter in the computed heating rate points (fig. 15). The agreement with theory may be fortuitous under these conditions; however, the four measuring stations on the leading edge do show remarkable consistency. The reason for the low ratios shown for the data at 88.4 through 89.0 seconds cannot be ascertained with certainty. Possibly, the angles of attack and yaw are still sufficiently large to affect the measurements. As is shown subsequently, the angle of attack, although estimated to be fairly low, does have a noticeable effect on the relative levels of heating on the three flat faces up to about 89 seconds. The use of estimated angle of attack (modifying effective sweep angle) in computing theoretical values of leading-edge heating rates, however, had negligible effect at times after 88.4 seconds.

There are probably Mach number effects in the reduction with sweep parameter (the theory of ref. 10, for example), which are not accounted for by the method of prediction used herein. These effects would, however, be expected to raise the predicted level at the lower Mach numbers, or increase the difference between prediction and experiment.

The data for times after 89 seconds show quite good agreement with the theory. At these times the measured heating rates are highest and the data would be expected to have the most accuracy.

The data of figure 16 would indicate that the reduction in heat transfer with sweep is proportional to $(\cos \Lambda)^{3/2}$. If $\cos \Lambda$ (which has also been proposed as the proper value for this parameter) had been

used instead of $(\cos \Lambda)^{3/2}$ in computing the theoretical heating rates, the level predicted by the theory would have been 1.93 times higher than the theory level shown in figure 16. For the data of this test, the use of $\cos \Lambda$ would therefore result in a large overestimate of the leading-edge heating rate. (It should be noted that the difference between $\cos \Lambda$ and $(\cos \Lambda)^{3/2}$ is of appreciable magnitude only at the higher values of sweep angle, say greater than 40°.)

From the data of the test, it would appear that the heating of a swept cylindrical leading edge of a glide missile wing can be predicted with reasonable accuracy by using the Fay and Riddell theory as modified herein. Since this theory is very easy and straightforward to evaluate (when Lewis number is assumed to be 1.0 and when perfect-gas relations are used), it would seem to be a useful relation for engineering calculation of leading-edge heating. The discussion presented in the following section should, however, be considered in an evaluation of its merits.

Factors Arising from Model Geometry

Before comparing the data of this experiment with other experiments and theories, it is desirable first to consider some factors peculiar to this test. The leading edge of the model is not a true cylindrical leading edge in that it is formed by the radius at the intersection of two sides of the pyramidal nose. (See fig. 3.) The precise effect of this geometry on the leading-edge stagnation-line heat-transfer rates is difficult to evaluate. Since the sonic line on a cylinder is about 45° from the stagnation line, and since the point of tangency of the side and leading edge of the configuration tested was 60° from the stagnation line, it would appear that the lack of a complete cylinder at the leading edge would not significantly alter the test results from those that would be expected for a swept infinite cylinder. However, consideration of the shock structure around the test nose complicates the analysis.

This shock structure is difficult to determine without visual flow tests of the configuration flown. A rough qualitative analysis can be made, however. The shock over the 8° flat surfaces of the simulated wing would, of course, be detached from the surfaces. The juncture of these shocks at the edges of the surfaces (the simulated wing leading edge) would probably alter the shock around the leading edge and give it somewhat different curvature and detachment distance than would exist on a yawed infinite cylinder. Since the flow-deflection angle is low, it is believed that this effect would be small, particularly at the higher Mach numbers when the shock would lie quite close to the flat surface. The shock formation over the nose can also be considered from another point of view. It can be reasoned that the shocks over

the simulated leading edges would be approximately the same as the conical shock occurring on a cone circumscribed about the pyramid, or a 13.5° half-angle cone. The shock over this cone would also lie close to the surface, particularly at the higher Mach numbers, and its effects on changing the heat transfer from the value that would be expected on a yawed infinite cylinder are believed to be small.

The effect of thse shocks would probably be to cause variation in heat transfer along the length of the leading edge. (The blunt-nose tip would induce a normal shock at the nose which would also tend to produce the same effect.) The data of figure 16 show small, and no consistent, variations with length along the leading edge; the small differences in heating rates between the measuring stations at any given time are within the overall accuracy of the data. This fact, plus the generally good agreement with the theory, is believed to warrant the above statement that the shock formation over the test nose does not significantly alter the heating rates measured from those that would occur on a swept infinite cylinder. The argument that the agreement between theory and experiment may be fortuitous cannot, however, be rigorously disproved.

The use of an effective leading-edge thickness less than the physical thickness in the data reduction for the leading edge (see data reduction section) reduced the computed heating rates from those computed by use of the actual physical thickness. If the actual thickness were used, the experimental rates would be about 30 percent higher at the higher values of time presented and higher by somewhat lesser amounts at the earlier times; the change would be negligible for the data presented before 88.4 seconds. The use of the effective thickness rather than the actual thickness is considered the more reasonable procedure. The agreement between theory and experiment would still be fairly reasonable, however, if the thicker wall were used in the data reduction.

Comparison With Other Theories and Experiments

Theroetical heating rates were also computed by the theory of reference 11 $\left(\text{where the parameter } \frac{E}{\sqrt{C}} \text{ (eq. 10(a), ref. 11) was chosen to be 1.0 which is equivalent to assuming that conductivity and viscosity of air vary in the same way with temperature}\right)$. Heating rates were computed by using both $\frac{T_{aw}}{T_s} = 1.0$ and $\frac{T_{aw}}{T_s} = 0.87$. (This value of "recovery factor" for a sweep angle of 75° was obtained from ref. 12.) The heating rates thus computed were, respectively, slightly higher than and slightly lower than the rates computed from the modified Fay and Riddell theory. The theory of reference 11 predicts, for $M = \infty$ (or practically for $M \gtrsim 7$) a variation of heat-transfer coefficient with

sweep proportional to $(\cos \Lambda)^{3/2}$; the theory predicts a lesser reduction with sweep for lower Mach numbers (as does the theory of ref. 10). The experimental results of reference 11 also show a reduction in heat-transfer rates due to sweep proportional to $(\cos \Lambda)^{3/2}$; the data were obtained, however, at a maximum sweep angle of about 45°.

The experimental data of reference 13 also indicate that the heating rate is decreased by $(\cos \Lambda)^{3/2}$ for sweep angles up to 45°. (There is considerable scatter in the data, but the general trend is a reduction proportional to $(\cos \Lambda)^{3/2}$.) However, the data for a 70° sweep angle show a reduction more nearly proportional to $\cos \Lambda$. The reason for this change in trend is not readily apparent. It should be noted that the data of reference 13 were obtained at low free-stream Reynolds numbers (315 to 2,100).

Experimental data reported in reference 14 indicate that the reduction in heating rate with yaw angle is proportional to $(\cos \Lambda)^{3/2}$. The data were obtained at a nominal Mach number of 10.4 and at sweep angles up to 70°. However, these test results are subject to a possible limitation in that they were obtained at Reynolds numbers so low that the possibility of the occurrence of slip flow during the test should be considered.

The experimental data of reference 12 indicate a reduction with sweep in heat-transfer coefficient which is proportional to $\cos \Lambda$. The reason for the reduced benefits of sweep in reducing leading-edge heating which is indicated by these data is not known. At least part of the disagreement is attributable to the fact that the data of reference 12 are heat-transfer coefficients. Heating rates would show a greater benefit of sweep in alleviation of heating than do heat-transfer coefficients because of the influence of recovery factor variation with sweep. Recovery factor decreases with sweep, hence, T_{aw} and the resulting forcing function $T_{aw} - T_w$ also decrease with increasing sweep angle.

The theory of reference 10 also shows that, for high Mach numbers ($M \geqq 7$), sweep reduces the heat-transfer coefficients by a factor of about $(\cos \Lambda)^{3/2}$. As was previously mentioned, this theory (and others) also shows a Mach number effect on the reduction with sweep parameter; at lower Mach numbers the effect of sweep is theoretically not so beneficial. The experimental data of the test reported herein show different trends. The reason for this difference is not readily apparent; it might possibly lie in inaccuracies in the data at the lower Mach numbers ($M \approx 4$ at 86 and 87 seconds) and incorrect estimates of angle of attack for the data from $t = 88.4$ to 89.0 seconds (fig. 16).

Comparison With Theory for Data on the Flat Wing Surface

The experimental heating data on the flat surface of the glide missile wing are compared with theory in figure 17. The data are shown as reduced to local Stanton number. Local flow conditions were those computed for an 8° wedge and by use of total pressure losses through an oblique shock at the wedge leading edge. Real-gas effects on total temperature and specific heat were used, the viscosity was assumed to be proportional to $T^{0.76}$ and ideal-gas relations were used to compute the remaining flow conditions.

Theoretical Stanton numbers were computed from the theories of Van Driest (ref. 15). Adiabatic wall temperatures were computed by using recovery factors of 0.84 and 0.88 for laminar and turbulent flow, respectively. The laminar recovery factor was used in the reduction of experimental data.

The experimental data of figure 17 are shown as correlated by two different methods. In method 1 (figs. 17(a) to (c)) the data are plotted on the basis of length from the leading edge to the measuring station in a direction parallel to the wing center line. In method 2 (figs. 17(d) and (e)) the data are correlated on the basis of length along the rays from the model apex. There is, in general, better correlation by the first method (figs. 17(a) to (c)). The data indicate that the flow over the flat surface was probably laminar.

Data are shown in figure 17 for measuring stations on all three flat surfaces. The data for the sides opposite the main thermocouple array, shown as flagged symbols, scatter about the general level of the other data. The single flagged symbols are for thermocouples 13 and 23 and the double flagged symbols are for thermocouples 14 and 24 (see fig. 5). Time history comparisons of the data for thermocouples on all three sides are shown subsequently.

There is scatter in the data of figure 17, the points on or nearest the center line showing the greatest variations. Although it is probable that the simplified flow analysis used does not properly account for the effects of the actual pressure distribution on the heat transfer, it is possible that the anomalies in the data are due (at least in part) to inaccuracies in the basic data. The points showing the greatest scatter (both from the general trend at any one time and in self-consistency at the various times) are, in general, at measuring stations having the lowest heating rates. The exception to this trend is the point farthest forward and outboard on the surface (thermocouple 3). The problem at this station may be one of conduction correction. Since adequate temperature distributions were not obtained at the longitudinal station on which this thermocouple was located, the same correction was applied to thermocouple 3 that was applied to thermocouple 9.

The points showing the most deviation from theory are at $t = 88.4$ and 88.6 seconds, where there is still some angle of attack. The use of the estimated angles of attack in computing local flow conditions, however, shows small effect on the heat transfer due to angle of attack (as was true for the leading-edge data shown in the previous section).

It does appear, however, at least for the conditions of this test, that the heat transfer to the windward surface of a highly swept glide rocket wing at moderate angles of attack can be predicted with fair accuracy by the use of the Van Driest theory with Reynolds number based on distance from the leading edge parallel to the wing center line (method 1), and using appropriate local flow conditions.

It is interesting to note that, for this test, the computed laminar heat-transfer rates on the wing surface were not much different (about 5 percent less) when local flow conditions were based on losses through a normal shock at the wedge leading edge instead of assuming an oblique shock at the wedge leading edge. Therefore, for this test the agreement between theory and experiment would not change significantly if either type of local flow conditions were used.

At $t = 91$ seconds (or $M = 14.4$), laminar Stanton numbers were calculated for the stations on the windward surface by the method of Van Driest (ref. 15). With local flow conditions computed as discussed previously (but with the wedge angle taken to be 8° plus the angle of attack of approximately 12°), theoretical heating rates were computed. These theoretical rates were of the same general magnitude as the measured rates. This agreement may very well have been fortuitous, since there is some uncertainty as to the validity of the angle-of-attack determination, and these data have therefore not been plotted.

Comparison of Data on the Three Faces

In addition to the main array of thermocouples on one face, additional thermocouples were placed at two longitudinal stations on the center line of each of the remaining two surfaces. The data from each of the three surfaces are compared in figure 18, both outside wall temperature and heat-transfer rates are shown for the portion of the flight commencing with third-stage ignition.

Up to the time of fourth-stage ignition ($t = 87.4$ sec) the data are in close agreement as would be expected; differences are due mainly to scatter in the basic data due to the low temperatures and heating rates during this time.

The angle of attack which occurs at fourth-stage ignition ($t = 87.4$ sec) affects the heating rates in a logical manner, the

windward side (measured by thermocouple 14) of the model showing the highest rates. There are noticeable differences between the windward side and the two leeward sides (measured by thermocouples 13 and 15). At about 88.8 to 89.0 seconds the heating rate on the windward side begins to decrease (as the angle of attack is small at these times) and approaches the level of the data for the remaining two sides. At about 89.5 seconds at fifth-stage ignition when the test vehicle again goes to a high angle of attack, the data for the three sides of the model again diverge and again the trends are as would be expected.

When the data of figure 18 are considered in comparison with the data of figure 12, note that the model has accelerated from a Mach number of 6 to a Mach number of 10 during the time interval from maximum angle of attack ($t \approx 88$ sec) to the time of maximum heating on the windward face ($t \approx 89$ sec). The maximum heating rates, therefore, would not be expected to occur at the same time as the maximum angle of attack.

CONCLUDING REMARKS

A free-flight rocket-model test of a simulated glide rocket indicates that for Mach numbers up to 10 and for the free-stream Reynolds number range of the test (2×10^6 at the rearmost thermocouple location on the flat surface and 0.3×10^5 based on leading-edge diameter):

1. Stagnation-line heat-transfer rates to a highly swept cylindrical leading edge of a glide missile wing can be approximated with reasonable engineering accuracy by the use of the three-dimensional Fay and Riddell theory modified to two-dimensional heating rates by the factor $\frac{1}{\sqrt{2}}$ and reduced by the three-halves power of the cosine of the sweep angle. (This latter factor is not in agreement with reductions suggested by some wind-tunnel results, which have indicated that the reduction in heating with sweep varies as the cosine of the sweep angle.)

2. For the highly swept flat surfaces of the glide vehicle investigated, the laminar heat transfer to the windward surface at moderate angles of attack can be approximated with reasonable engineering accuracy by the use of the laminar flat-plate theory of Van Driest by using wedge local flow conditions and basing Reynolds numbers on lengths from the surface leading edge parallel to the surface center line (rather than on length along rays from the apex of the swept surface.

Langley Aeronautical Laboratory,
National Advisory Committee for Aeronautics,
Langley Field, Va., June 27, 1958.

REFERENCES

1. Stoney, William E., Jr., and Swanson, Andrew G.: Heat-Transfer Measurements on a Flat-Face Cylinder in Free Flight at Mach Numbers Up to 13.9. NACA RM L57E13, 1957.

2. Bland, William M., Jr., Rumsey, Charles B., Lee, Dorothy B., and Kolenkiewicz, Ronald: Free-Flight Aerodynamic Heating Data to a Mach Number 15.5 on a Blunted Conical Nose With a Total Angle of 29°. NACA RM L57F28, 1957.

3. Bland, William M., Jr., Swanson, Andrew G., and Kolenkiewicz, Ronald: Free-Flight Aerodynamic Heating Data at Mach Numbers Up to 10.9 on a Flat-Faced Cylinder. NACA RM L57K29, 1958.

4. Rumsey, Charles B., and Lee, Dorothy B.: Heat-Transfer Measurements in Free Flight at Mach Numbers Up to 14.6 on a Flat-Faced Conical Nose With a Total Angle of 29°. NACA RM L57L03, 1958.

5. Hill, P. R.: A Method of Computing the Transient Temperature of Thick Walls From Arbitrary Variation of Adiabatic Wall Temperature and Heat-Transfer Coefficient. NACA TN 4105, 1957.

6. Fay, J. A., and Riddell, F. R.: Theory of Stagnation Point Heat Transfer in Dissociated Air. Jour. Aero. Sci., vol. 25, no. 2, Feb. 1958, pp. 73-85.

7. Rose, P. H., and Stark, W. I.: Stagnation Point Heat-Transfer Measurements in Dissociated Air. Jour. Aero. Sci., vol. 25, no. 2, Feb. 1958, pp. 86-97.

8. Lees, Lester: Laminar Heat Transfer Over Blunt-Nosed Bodies at Hypersonic Flight Speeds. Jet Propulsion, vol. 26, no. 4, April 1956, pp. 259-269.

9. Reshotko, Eli, and Cohen, Clarence B.: Heat Transfer at the Forward Stagnation Point of Blunt Bodies. NACA TN 3513, 1955.

10. Reshotko, Eli, and Beckwith, Ivan E.: Compressible Laminar Boundary Layer Over a Yawed Infinite Cylinder With Heat Transfer and Arbitrary Prandtl Number. NACA TN 3986, 1957.

11. Goodwin, Glen, Craugor, Marcus O., and Winkler, Ernest L.: Investigation of Local Heat-Transfer and Pressure Drag Characteristics of a Yawed Circular Cylinder at Supersonic Speeds. NACA RM A55H31, 1956.

12. Feller, William V.: Investigation of Equilibrium Temperatures and Average Laminar Heat-Transfer Coefficients for the Front Half of Swept Circular Cylinders at a Mach Number of 6.9. NACA RM L55F08a, 1955.

13. Eggers, A. J., Jr., Hansen, C. Frederick, and Cunningham, Bernard E.: Theoretical and Experimental Investigation of the Effect of Yaw on Heat Transfer to Circular Cylinders in Hypersonic Flow. NACA RM A55E02, 1955.

14. Cunningham, Bernard E., and Kraus, Samuel: Experimental Investigation of the Effect of Yaw on Rates of Heat Transfer to Transverse Circular Cylinders in a 6500-Foot-Per-Second Hypersonic Air Stream. NACA RM A58E19, 1958.

15. Van Driest, E. R.: The Problem of Aerodynamic Heating. Aero. Eng. Rev., vol. 15, no. 10, Oct. 1956, pp. 26-41.

TABLE I

MEASURED WALL THICKNESS

Thermocouple	Thickness, in.	Thermocouple	Thickness, in.
1	-----	13	0.047
2	0.043	14	.047
3	.043	15	.047
4	.046	16	.044
5	.043	17	.045
6	.044	18	.046
7	.047	19	.046
8	.044	20	.046
9	.044	21	.045
10	.045	22	.047
11	.046	23	.045
12	.046	24	.046

TABLE II.- VALUES OF MEASURED INSIDE TEMPERATURES FROM FAIRED CURVES

Time, sec	Temperature, °F, for thermocouple -																							
	1	2	3	4	5	6	7	8	9	10	11	12	13	14	15	16	17	18	19	20	21	22	23	24
83.0	200	198	189	205	200	210	214	210	214	218	221	220	221	219	220	214	219	224	224	227	216	220	218	215
84.0	200	197	192	204	201	208	213	208	212	218	220	220	220	218	218	215	218	221	224	226	215	219	216	215
85.0	200	199	197	202	209	209	212	213	214	220	220	219	220	218	222	220	220	225	225	225	215	220	216	216
86.0	200	222	210	205	232	216	216	230	220	224	222	220	224	223	225	239	225	230	230	230	219	222	219	220
86.2	202	229	215	206	238	218	218	237	223	225	224	221	225	224	226	246	227	231	231	231	221	223	220	221
86.4	203	236	221	207	244	220	220	244	225	226	225	223	227	226	228	252	229	233	234	233	223	224	223	223
86.6	204	244	227	209	249	223	223	250	228	228	226	224	228	228	230	256	232	235	235	235	224	225	224	224
86.8	205	250	232	212	255	226	225	257	231	230	227	225	230	230	233	263	235	236	237	236	225	227	224	225
87.0	206	258	236	214	259	230	228	264	235	231	229	227	233	234	235	268	238	238	238	237	226	227	225	226
87.2	207	265	240	215	263	234	229	268	237	233	231	229	234	237	237	273	240	240	239	238	227	228	226	227
87.4	209	270	243	217	266	236	230	272	240	235	233	231	236	240	240	276	243	242	240	239	229	230	229	228
87.6	211	273	246	220	269	240	233	274	243	235	235	234	238	245	243	277	246	243	240	240	230	231	231	230
87.8	213	275	247	225	270	244	234	275	245	237	237	236	240	252	245	279	250	245	241	242	231	233	235	231
88.0	216	275	249	229	279	250	235	276	246	240	240	240	242	259	245	279	255	246	241	243	233	234	240	233
88.2	218	278	255	234	274	257	236	280	252	245	245	243	245	270	250	280	261	249	244	244	235	236	247	235
88.4	222	286	265	240	286	265	244	297	263	252	251	248	246	274	254	290	268	254	248	247	240	240	257	238
88.6	226	312	281	247	318	278	256	329	278	263	259	254	253	303	259	322	278	264	256	253	245	244	270	241
88.8	230	349	304	256	361	294	271	375	299	276	270	261	267	324	266	367	296	278	270	260	251	252	290	249
89.0	235	399	335	268	420	318	288	437	328	295	286	270	291	345	276	427	320	298	287	268	266	262	320	259
89.2	240	478	379	280	510	353	302	526	371	323	308	281	311	379	286	515	354	325	310	283	284	276	353	270
89.4	246	617	467	294	630	400	314	651	425	356	337	293	325	371	298	638	399	355	339	302	309	297	377	283
89.6	254	756	570	311	747	460	325	765	478	390	372	310	337	383	313	755	452	359	367	329	334	320	391	300
89.8	264	797	618	328	810	508	339	857	526	417	398	329	353	395	328	822	500	418	389	344	345	337	407	315
90.0	274	816	653	348	854	544	361	878	566	439	415	346	369	414	349	865	543	435	400	358	357	352	427	329
90.2	288	851	682	373	854	575	389	903	603	458	427	364	389	442	374	903	579	450	412	374	369	368	451	345
90.4	308	846	710	398	873	603	419	923	636	476	437	385	411	476	398	934	610	465	421	393	385	384	488	364
90.6	336	860	737	426	888	628	455	935	665	490	446	407	434	515	423	956	638	479	430	414	404	402	534	383
90.8	370	875	764	458	901	653	488	946	693	504	458	432	460	562	448	973	664	492	439	437	433	420	586	405
91.0	418	893	789	494	913	674	525	954	716	519	474	458	488	620	479	983	687	504	448	463	461	438	653	427
91.2	480	928	813	539	922	694	564	960	736	540	494	485	520	810	518	989	709	515	456	488	483	456	905	451
91.4	558	943	837	542	930	716	605	963	761	574	523	513	560	1120	583	990	731	526	468	517	505	474	1215	476

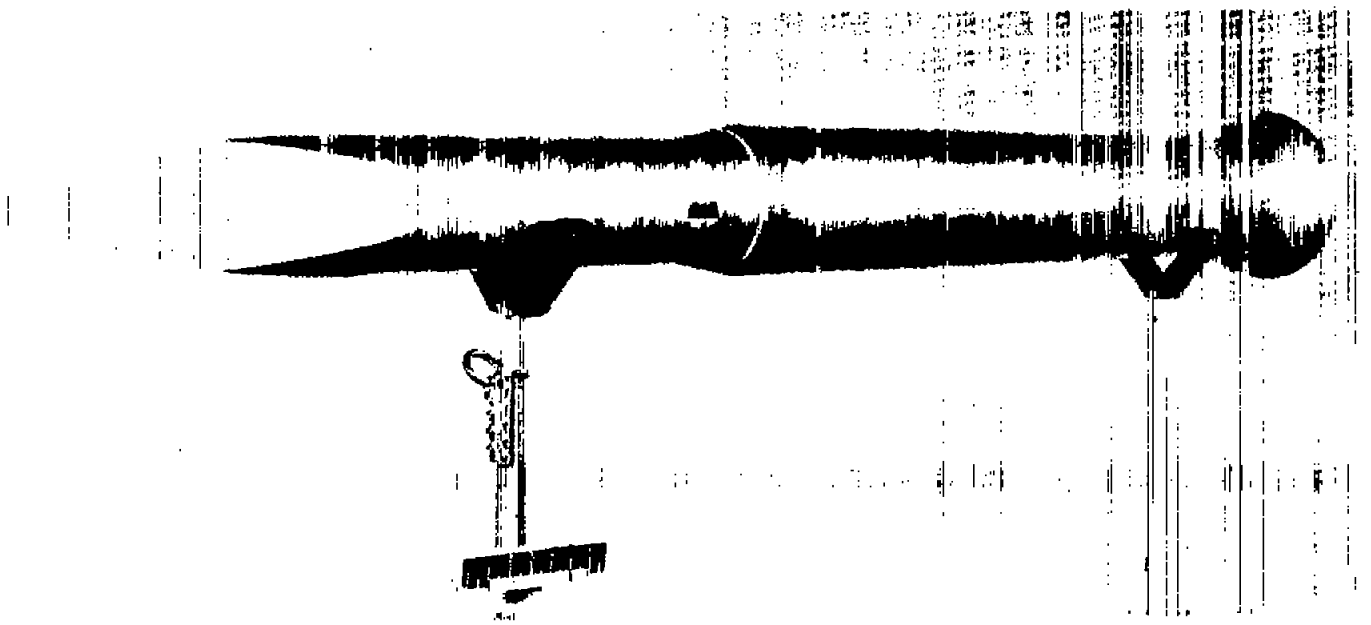

L-57-3645.1

Figure 1.- Photograph of test nose mounted on fifth stage.

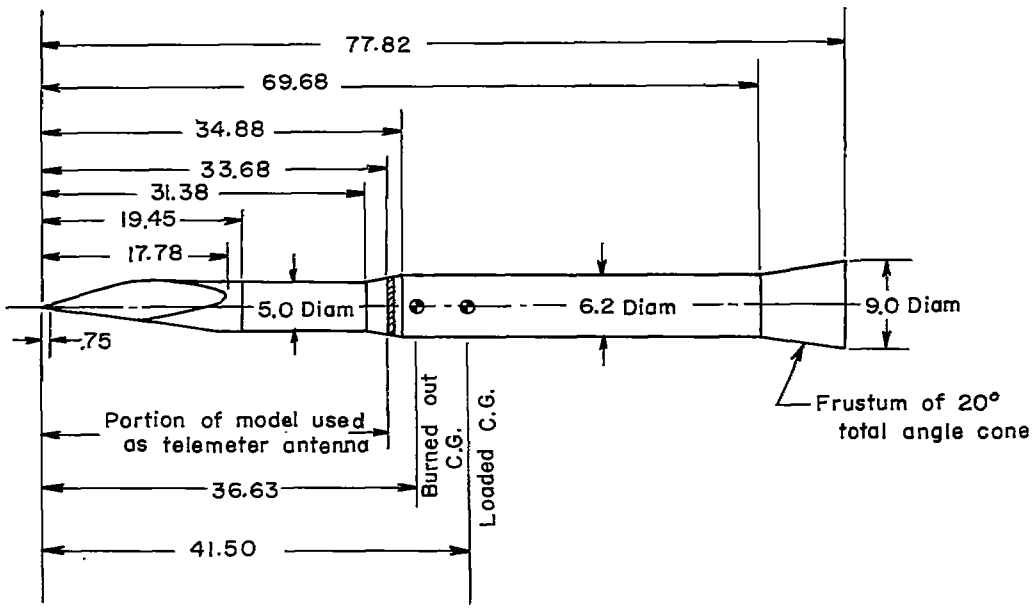

Fifth stage with test nose

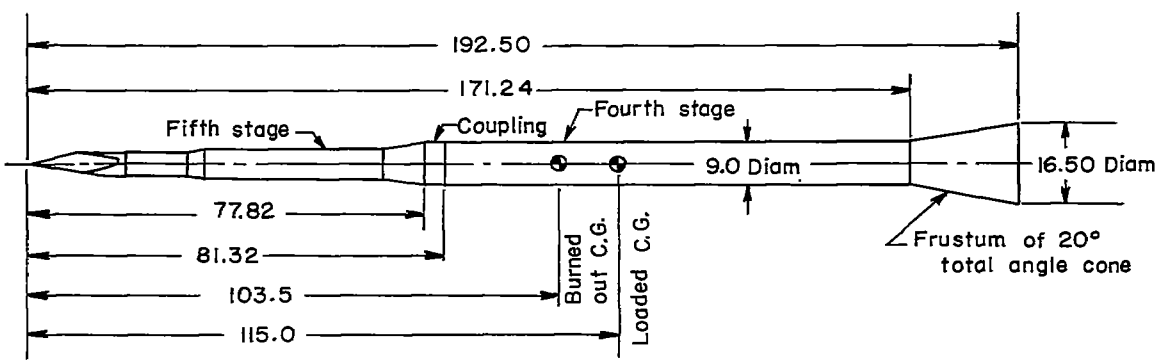

Fourth and fifth stage combination

Figure 2.- Sketch of test vehicle. Dimensions in inches.

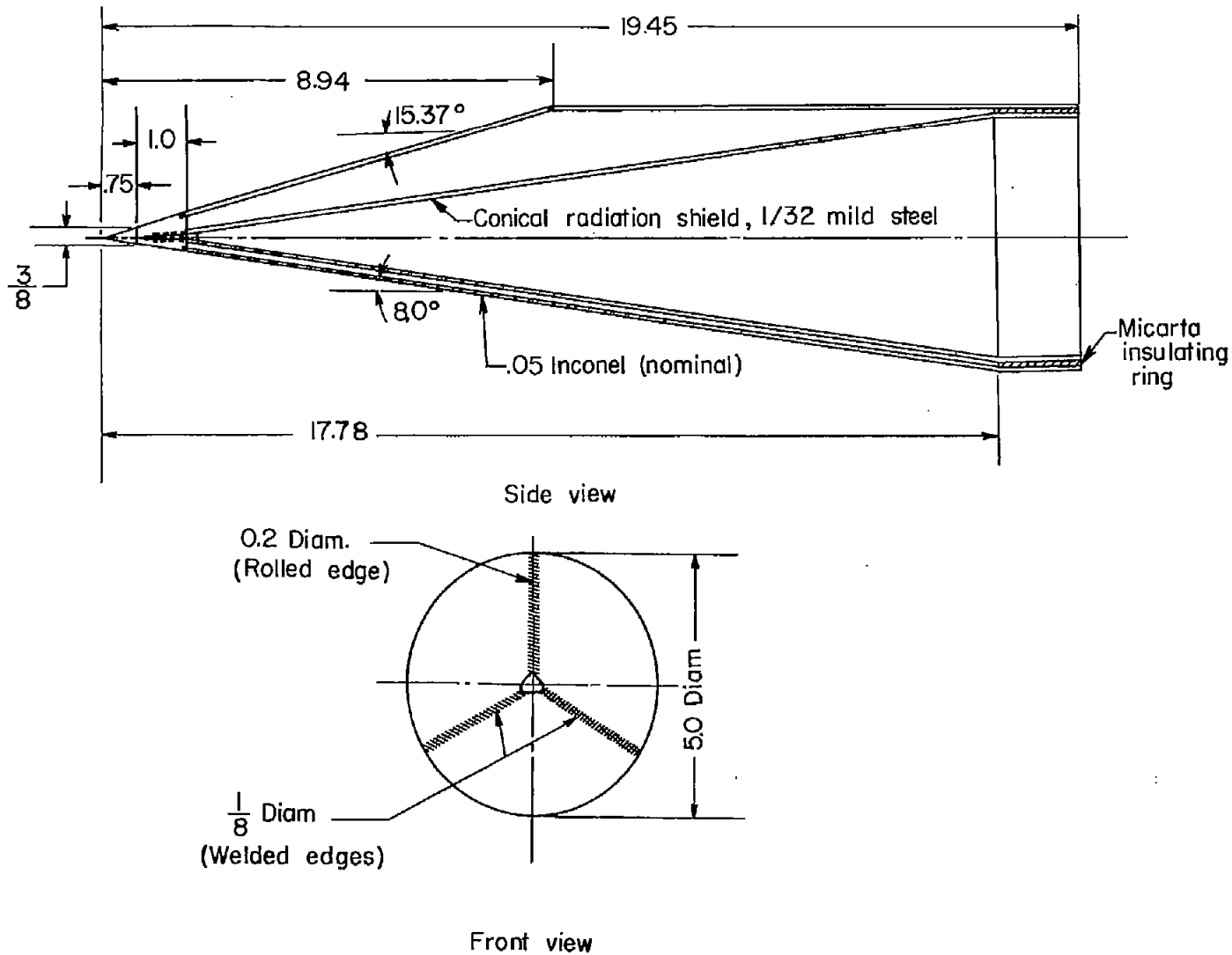

Figure 3.- Sketch showing nose construction. Dimensions in inches.

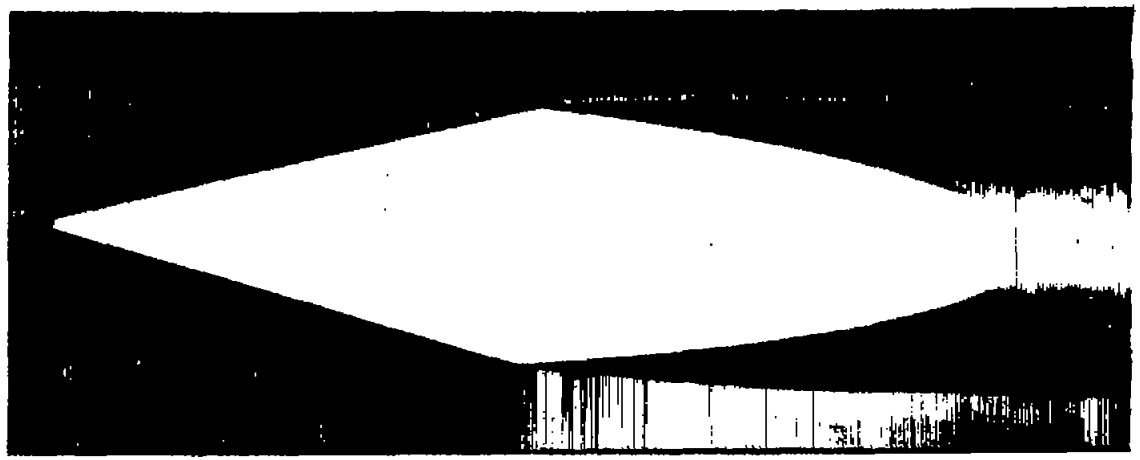

(a) Dots showing approximate thermocouple locations.

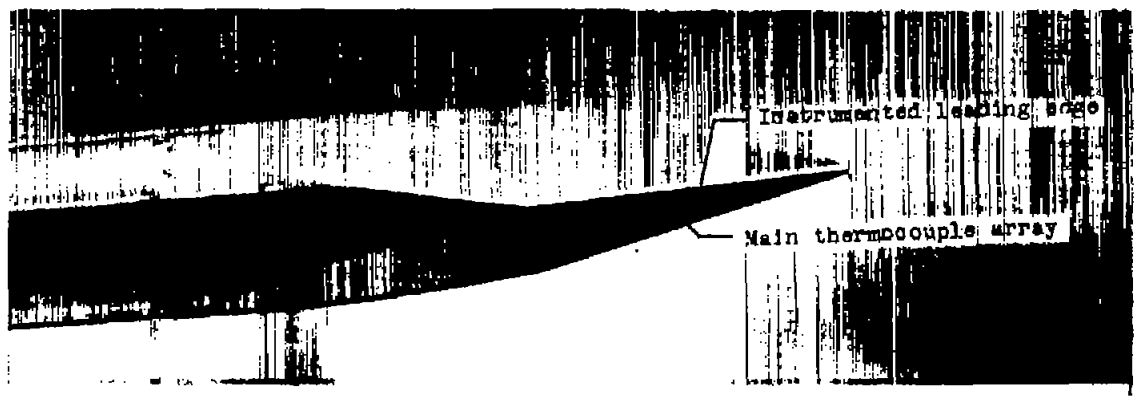

(b) Missile system mounted on launcher just prior to elevation for firing. L-58-1698

Figure 4.- Photograph of test nose.

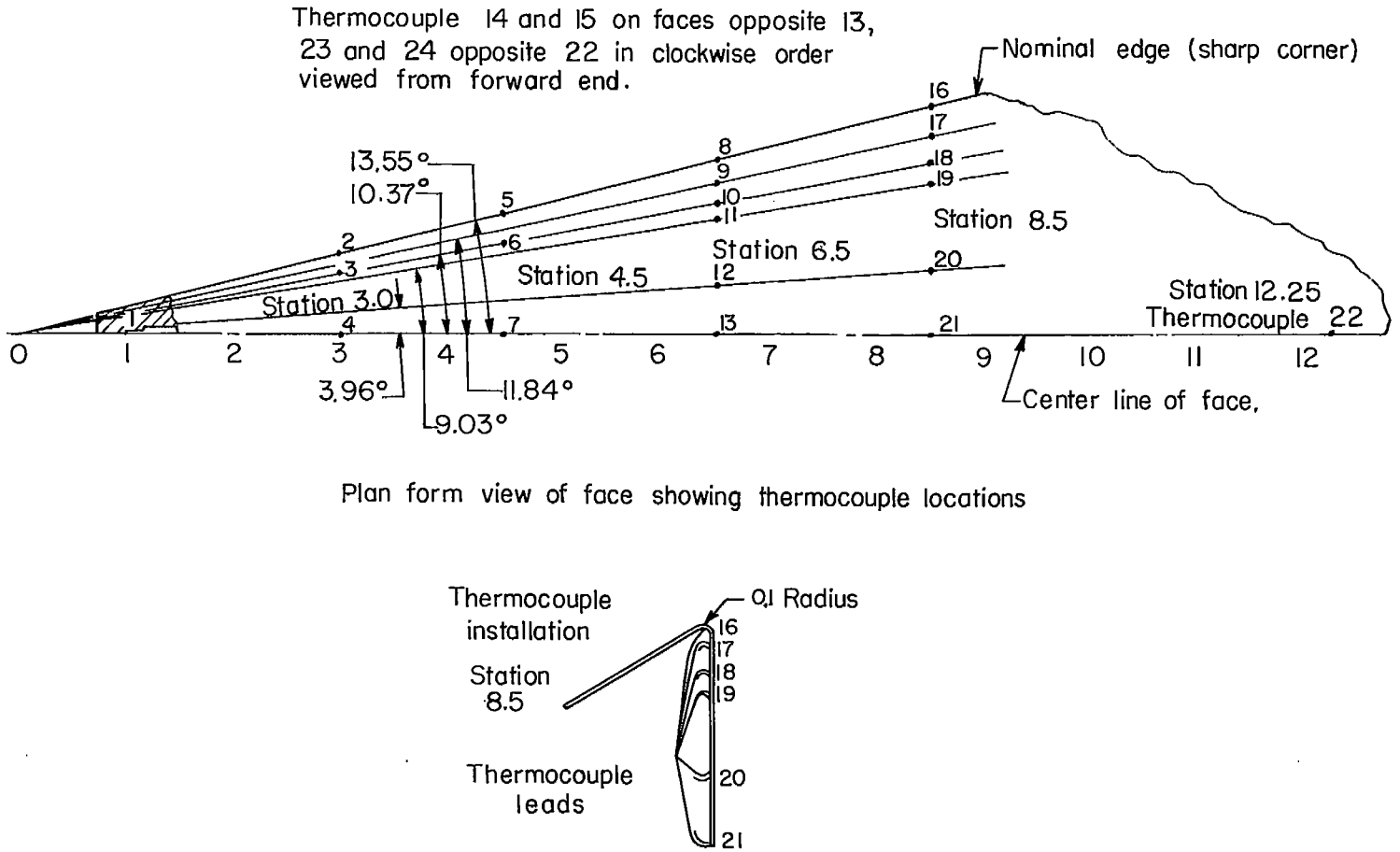

Figure 5.- Sketch of thermocouple locations on nose. Dimensions in inches.

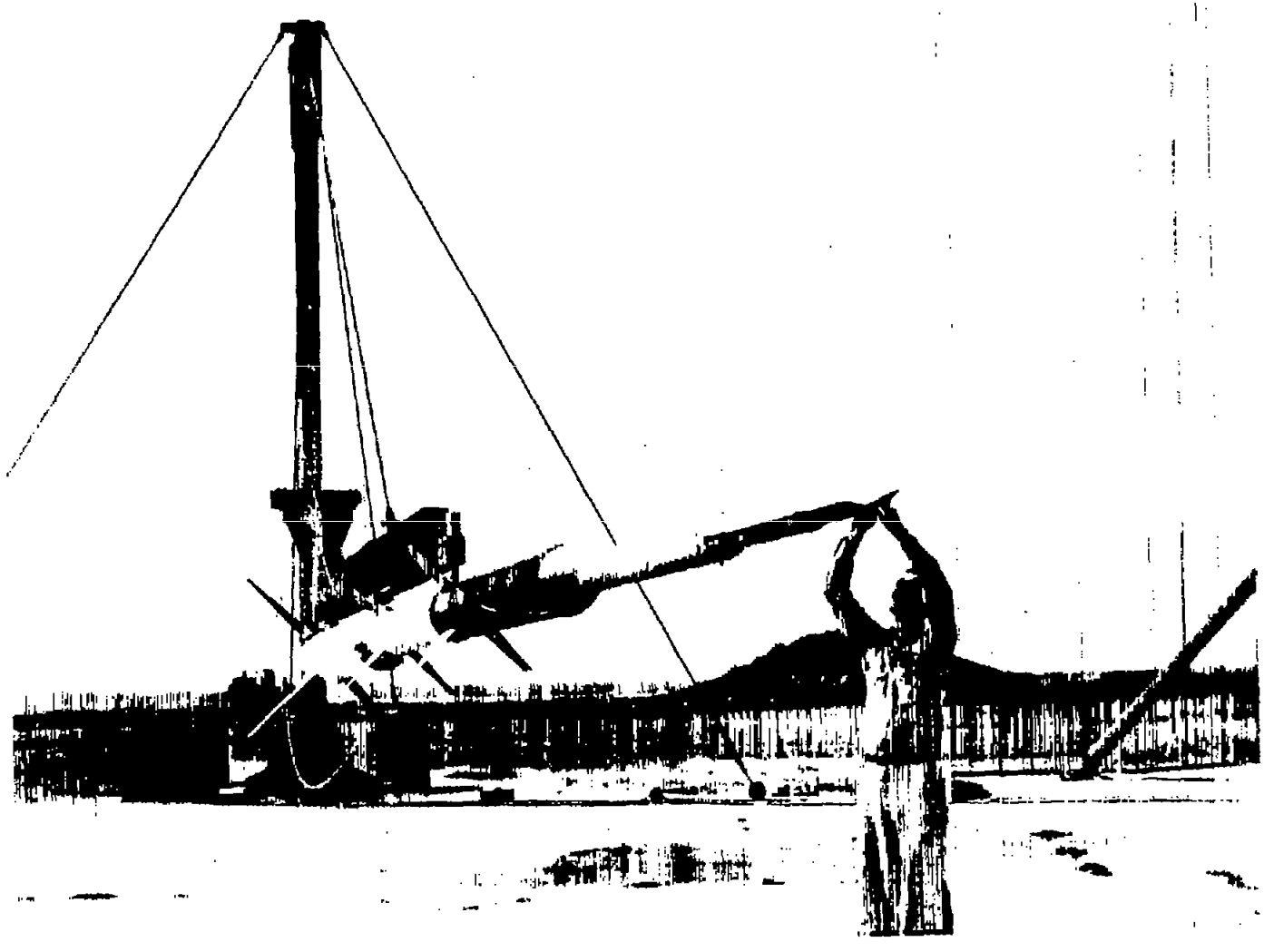

L-57-3838

Figure 6.- Missile system being prepared for launching.

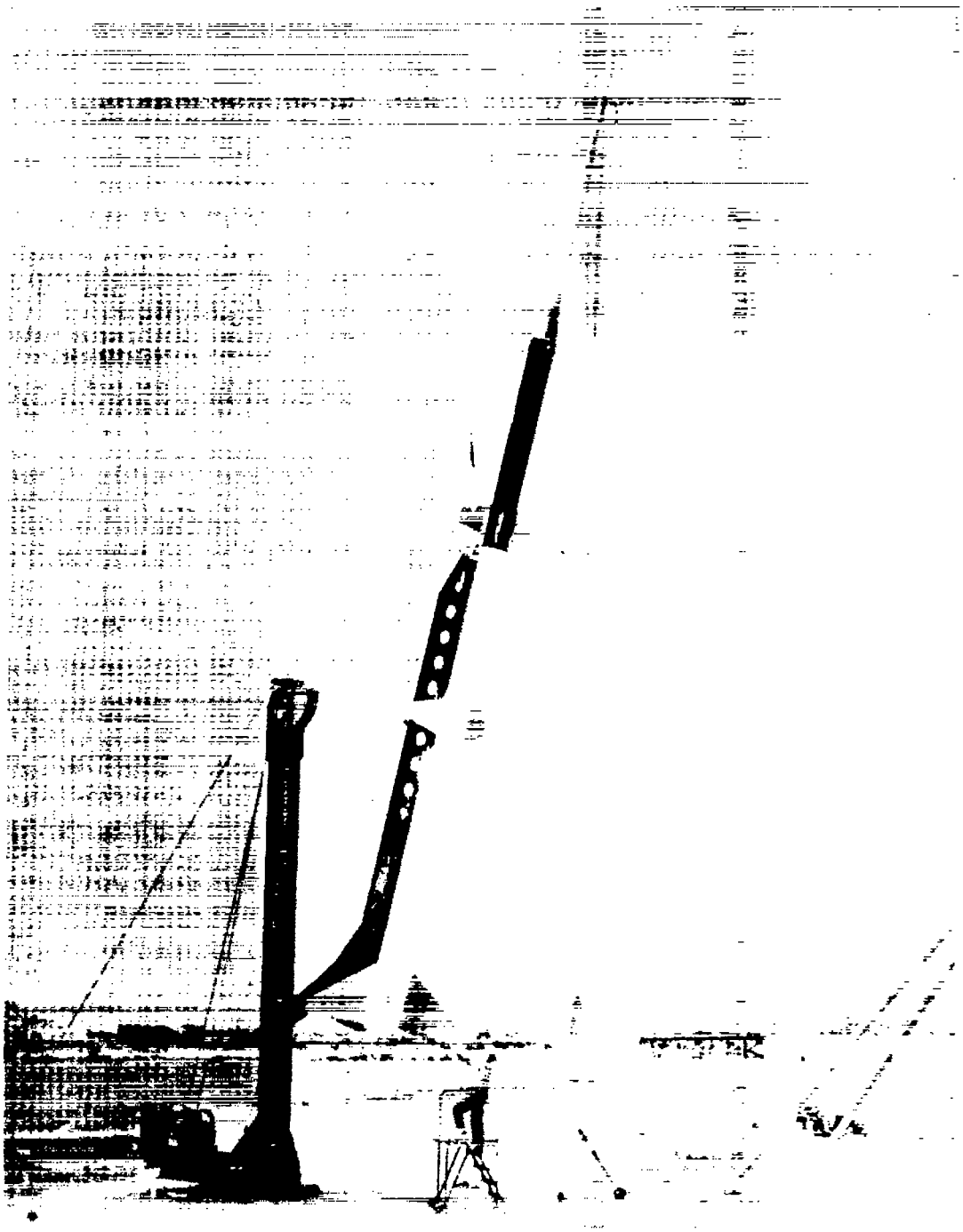

Figure 7.- Missile system elevated on launcher. L-57-3841

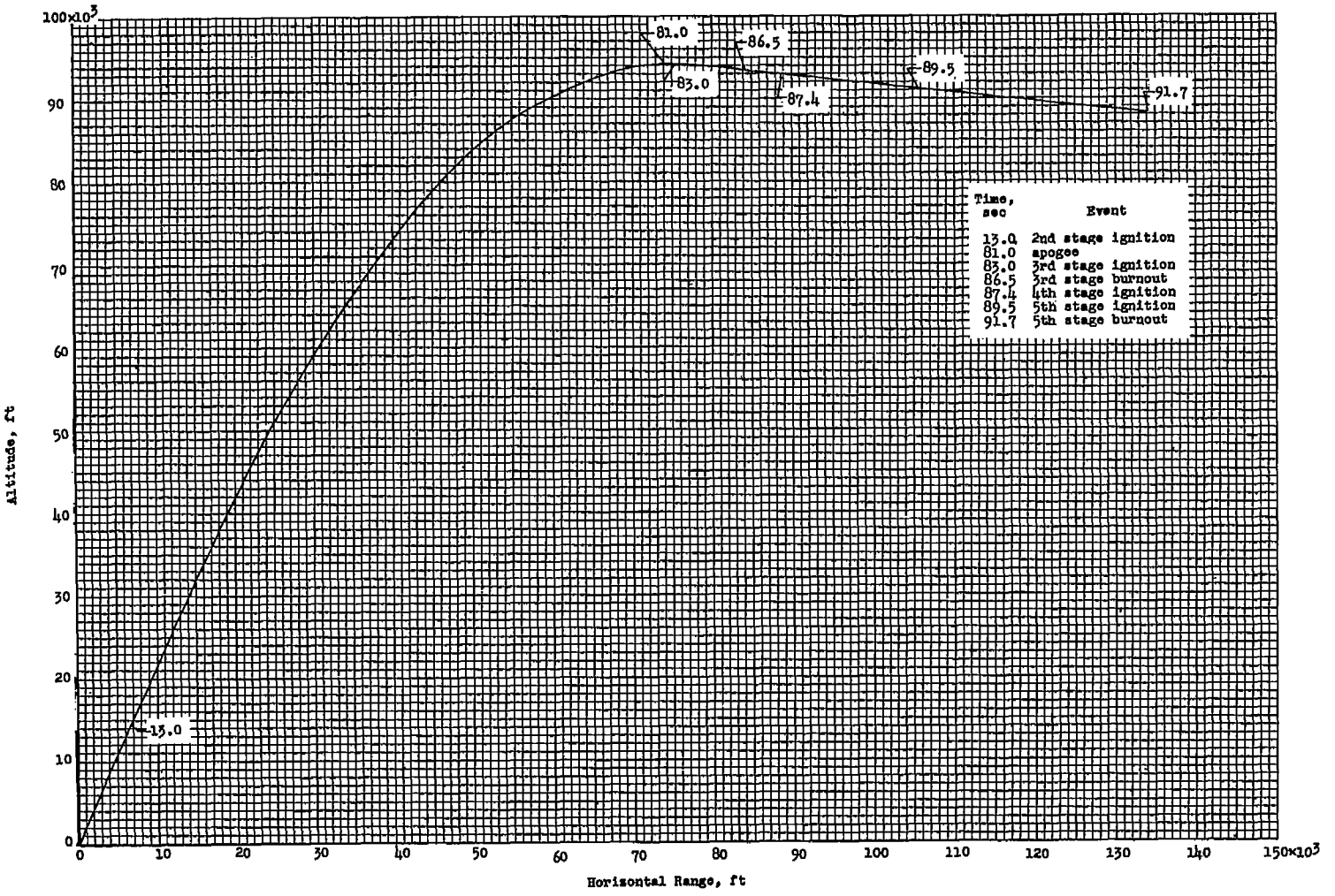

Figure 8.- Test vehicle flight path.

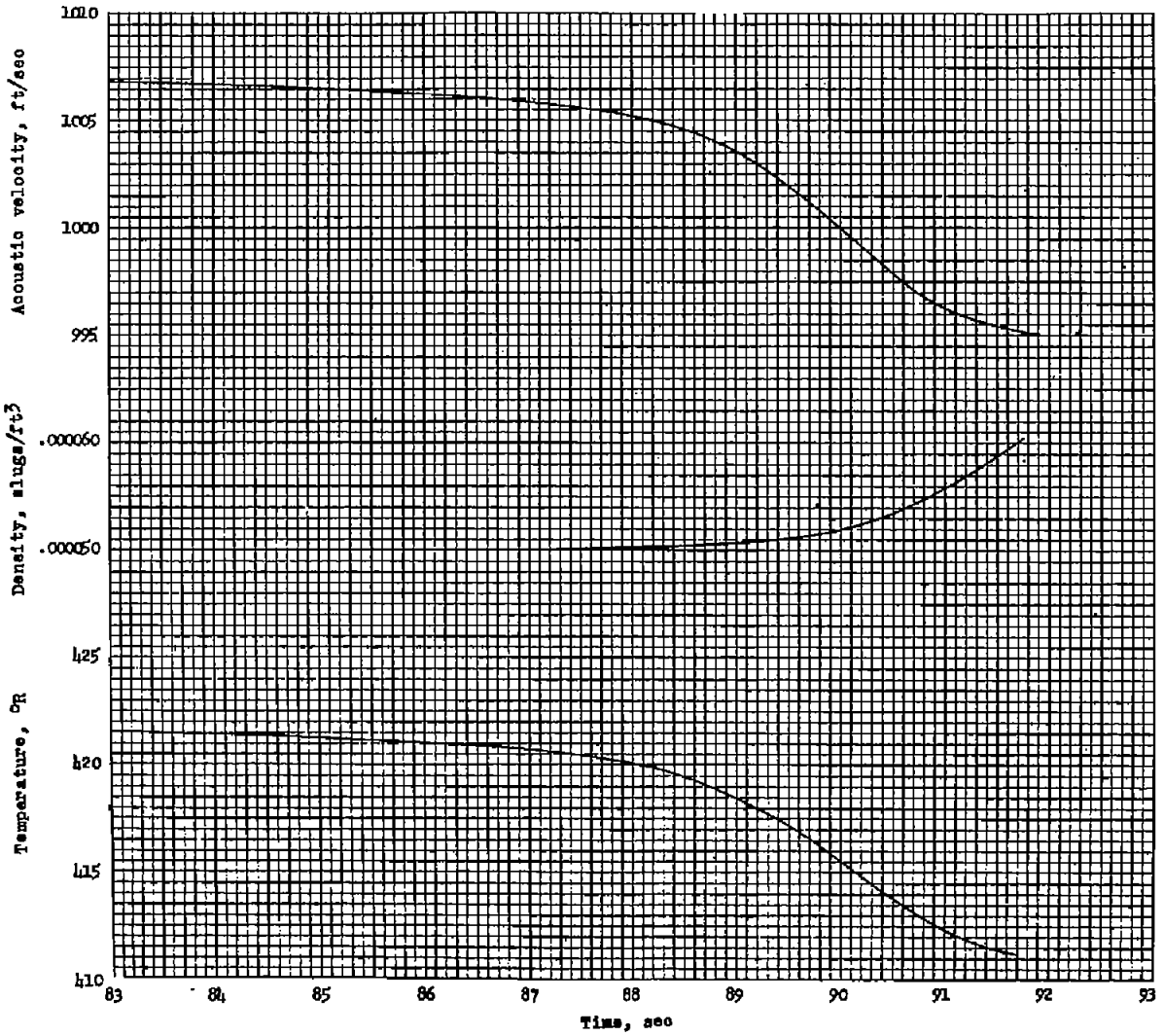

Figure 9.- Ambient atmospheric conditions from time of third stage ignition until fifth stage burnout.

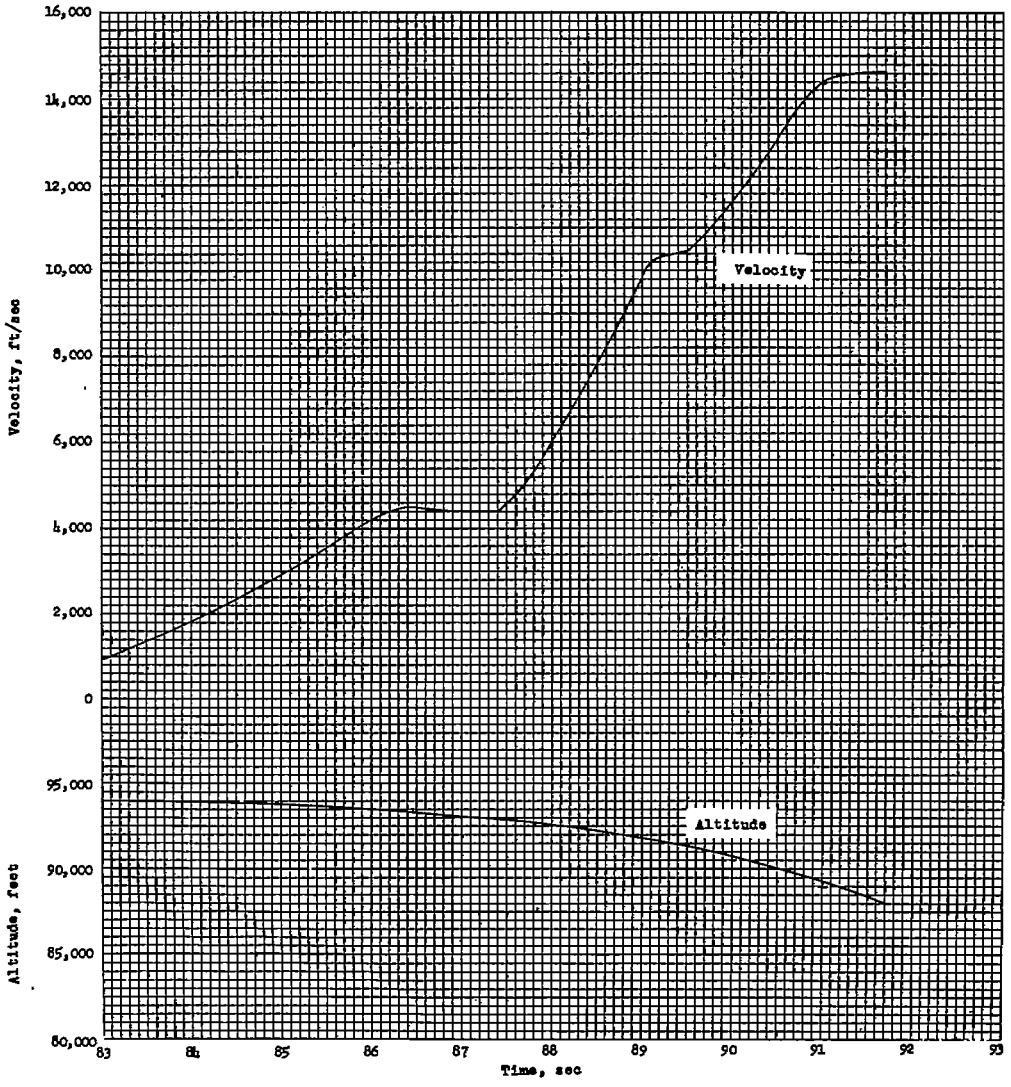

(a) Altitude and velocity.

Figure 10.- Test vehicle performance data from time of third-stage ignition until fifth-stage burnout.

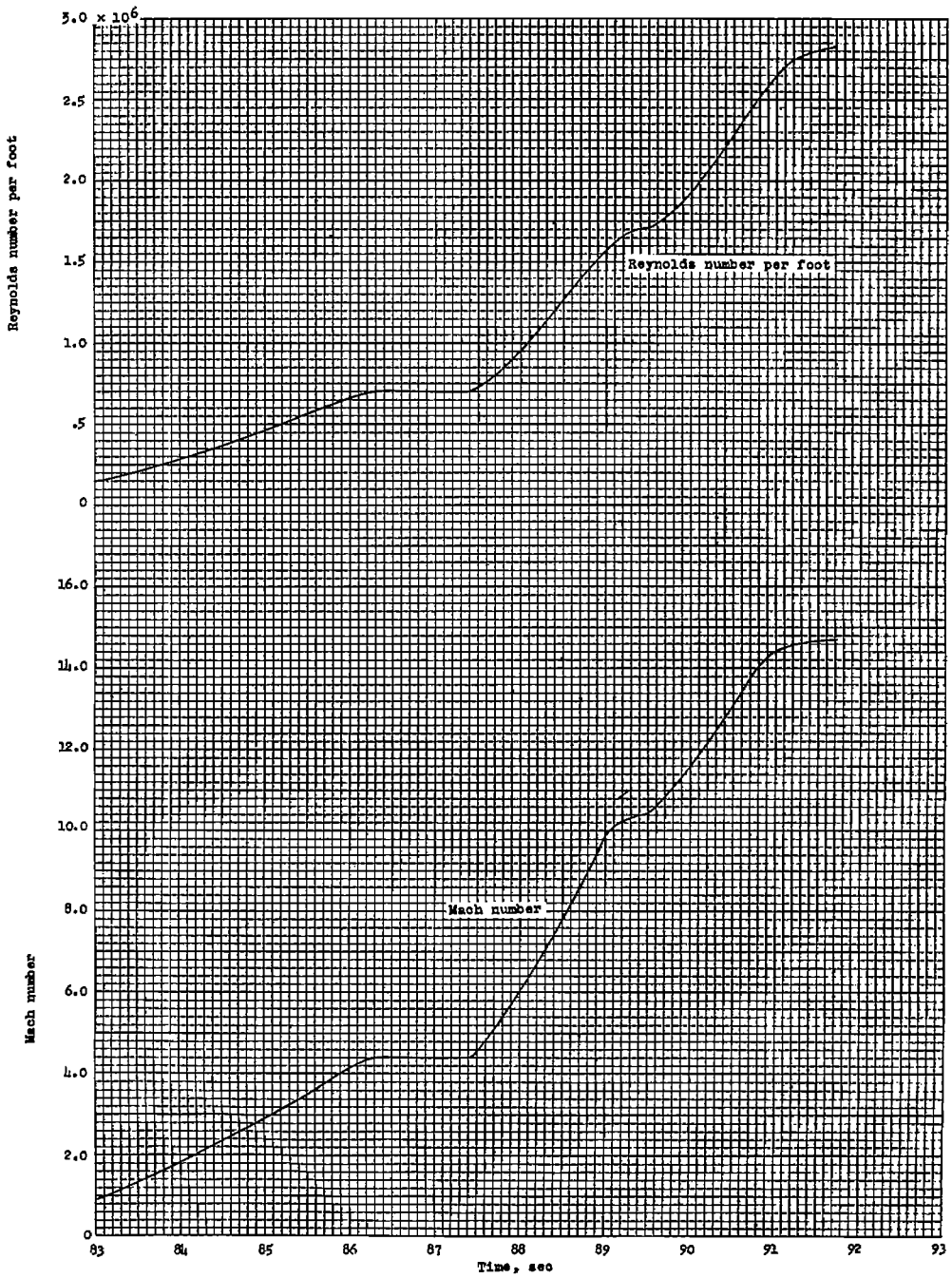

(b) Mach number and Reynolds number.

Figure 10.- Concluded.

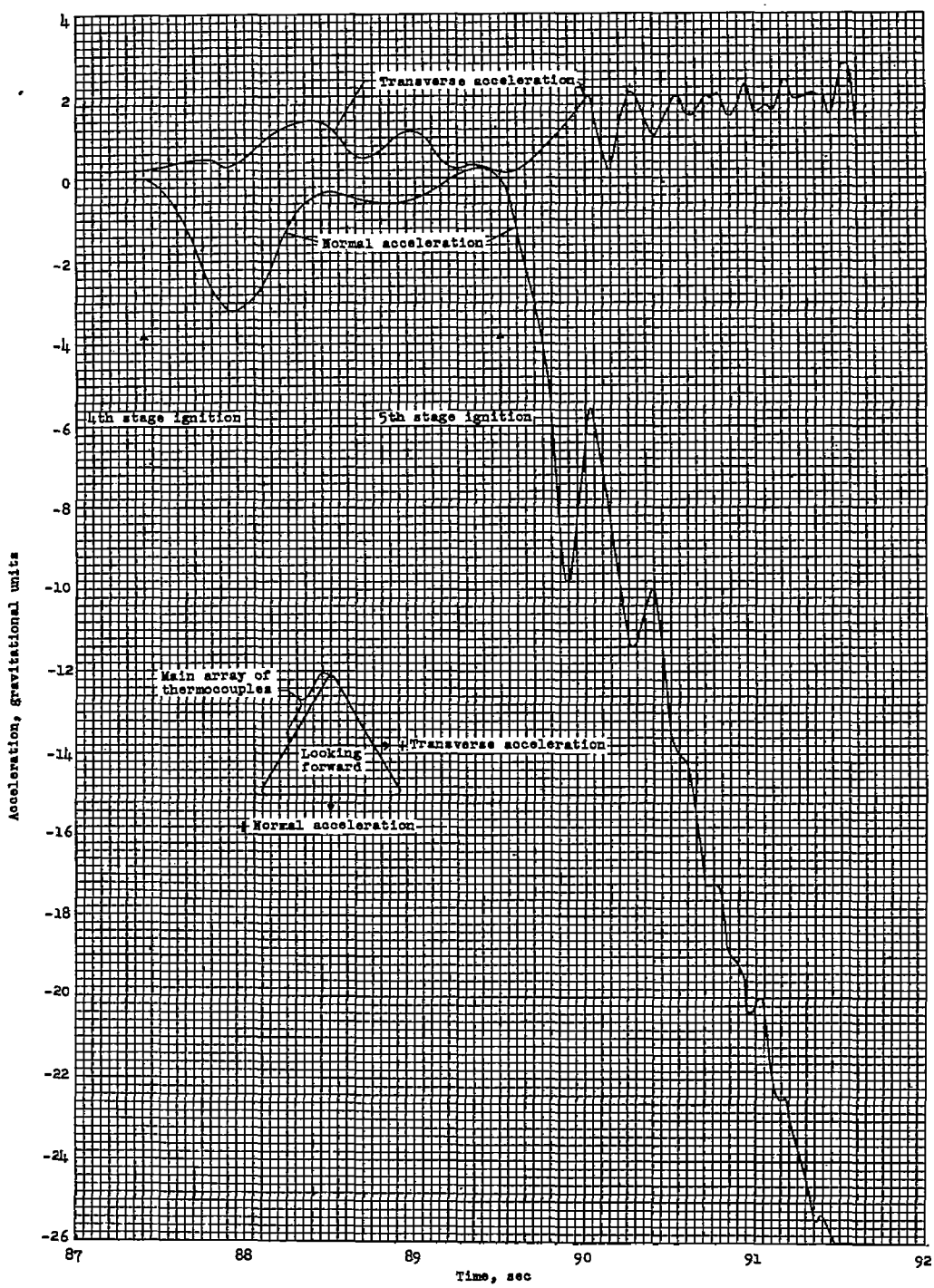

Figure 11.- Time histories of normal and transverse accelerations.

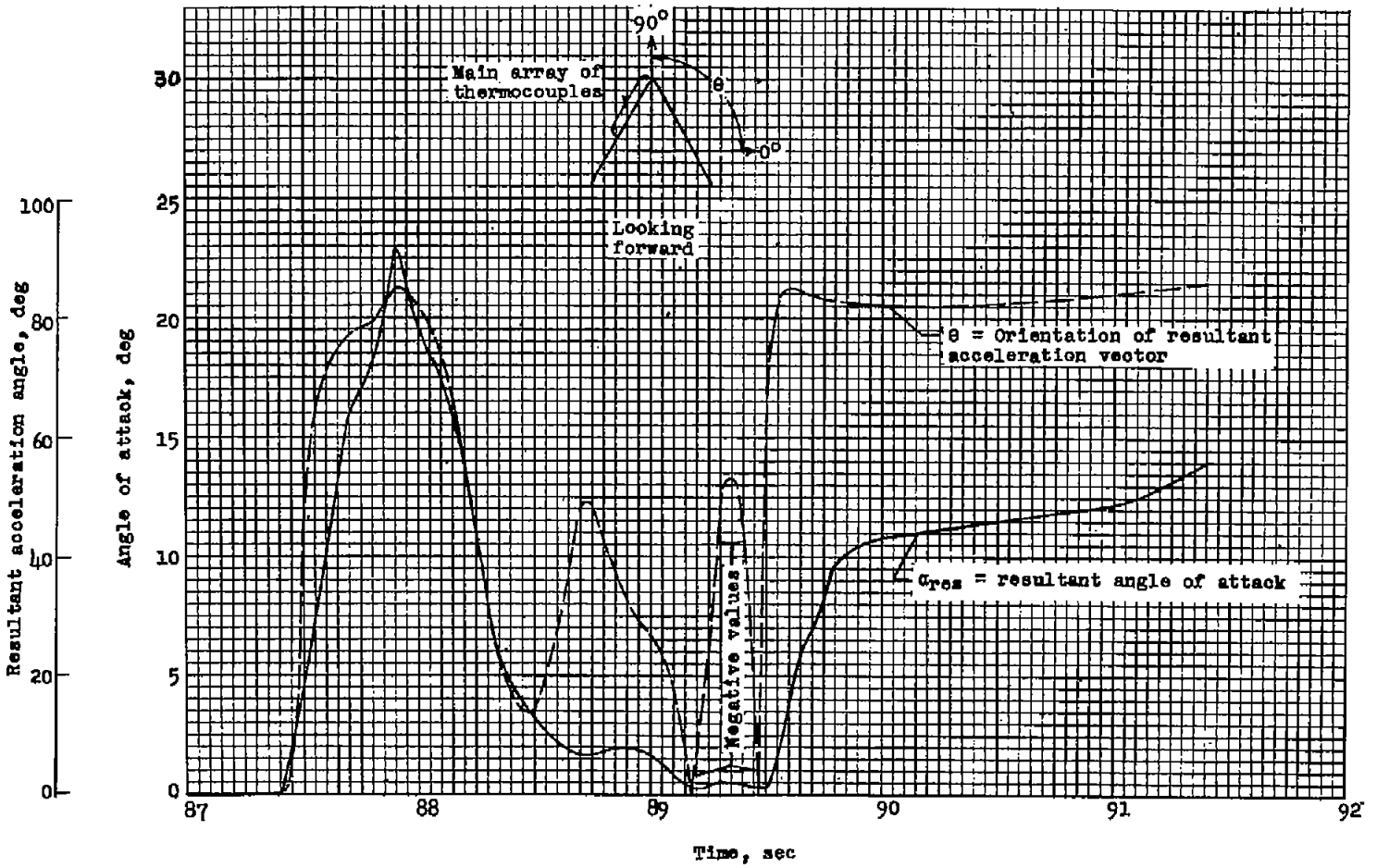

Figure 12.- Angle-of-attack time history.

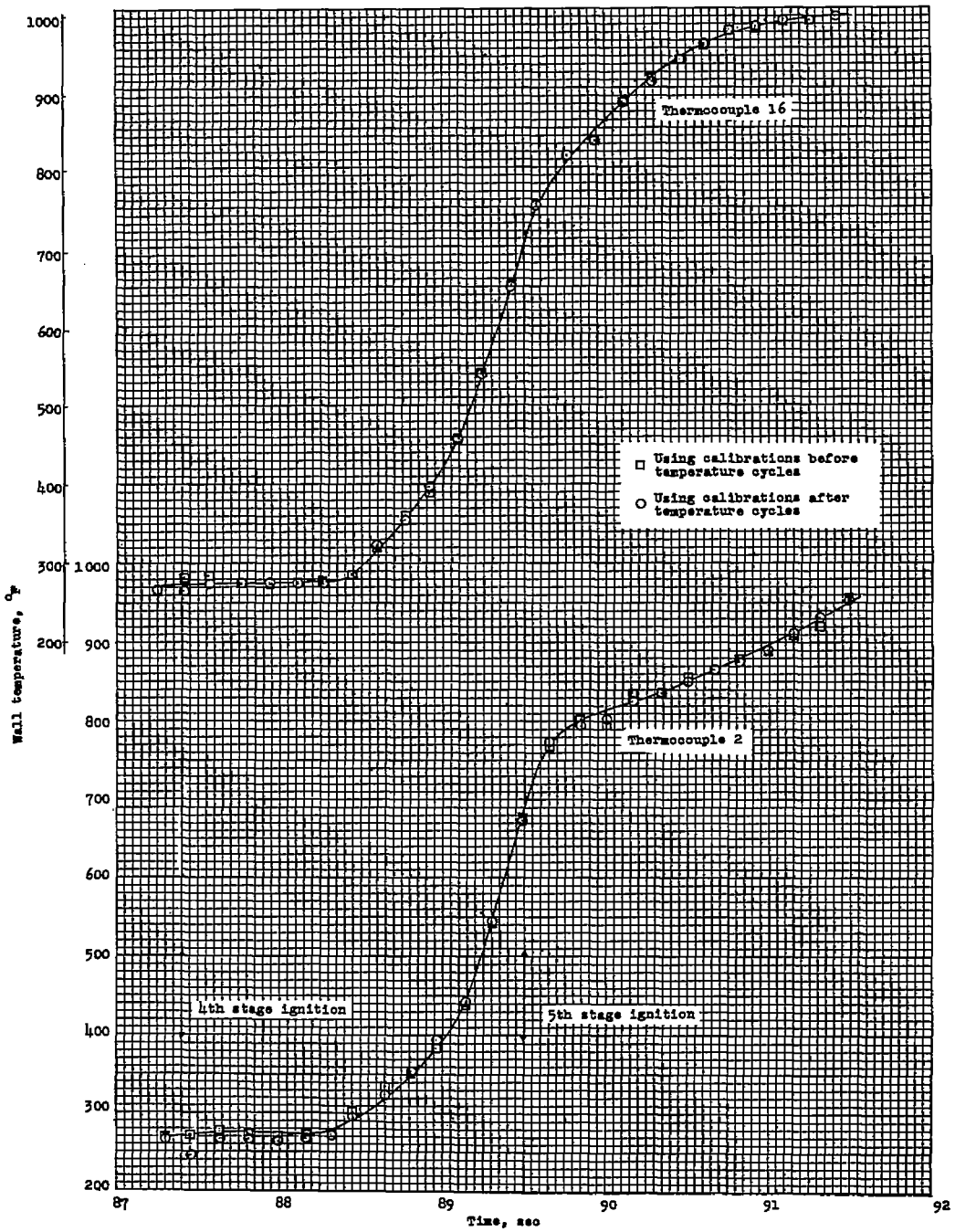

(a) Stations on leading edge.

Figure 13.- Typical time histories of measured temperatures.

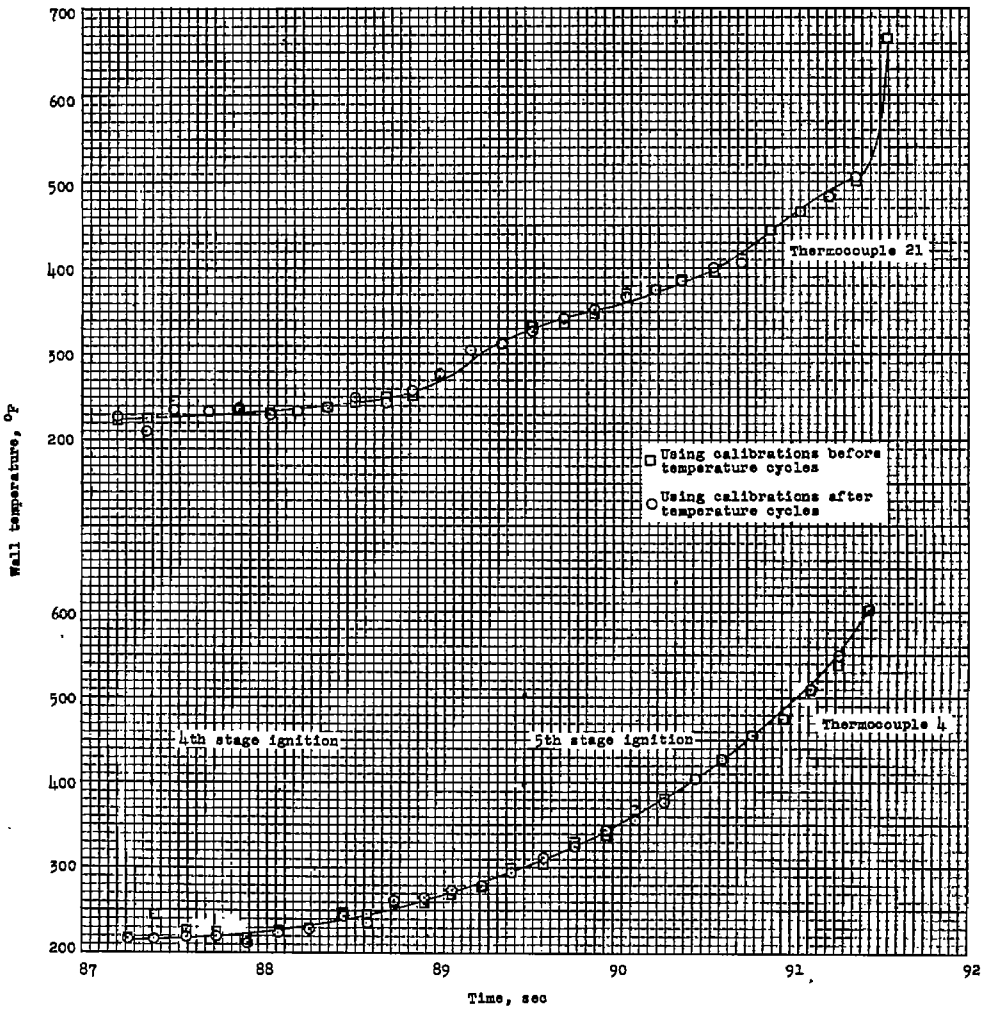

(b) Stations on surface center line.

Figure 13.- Continued.

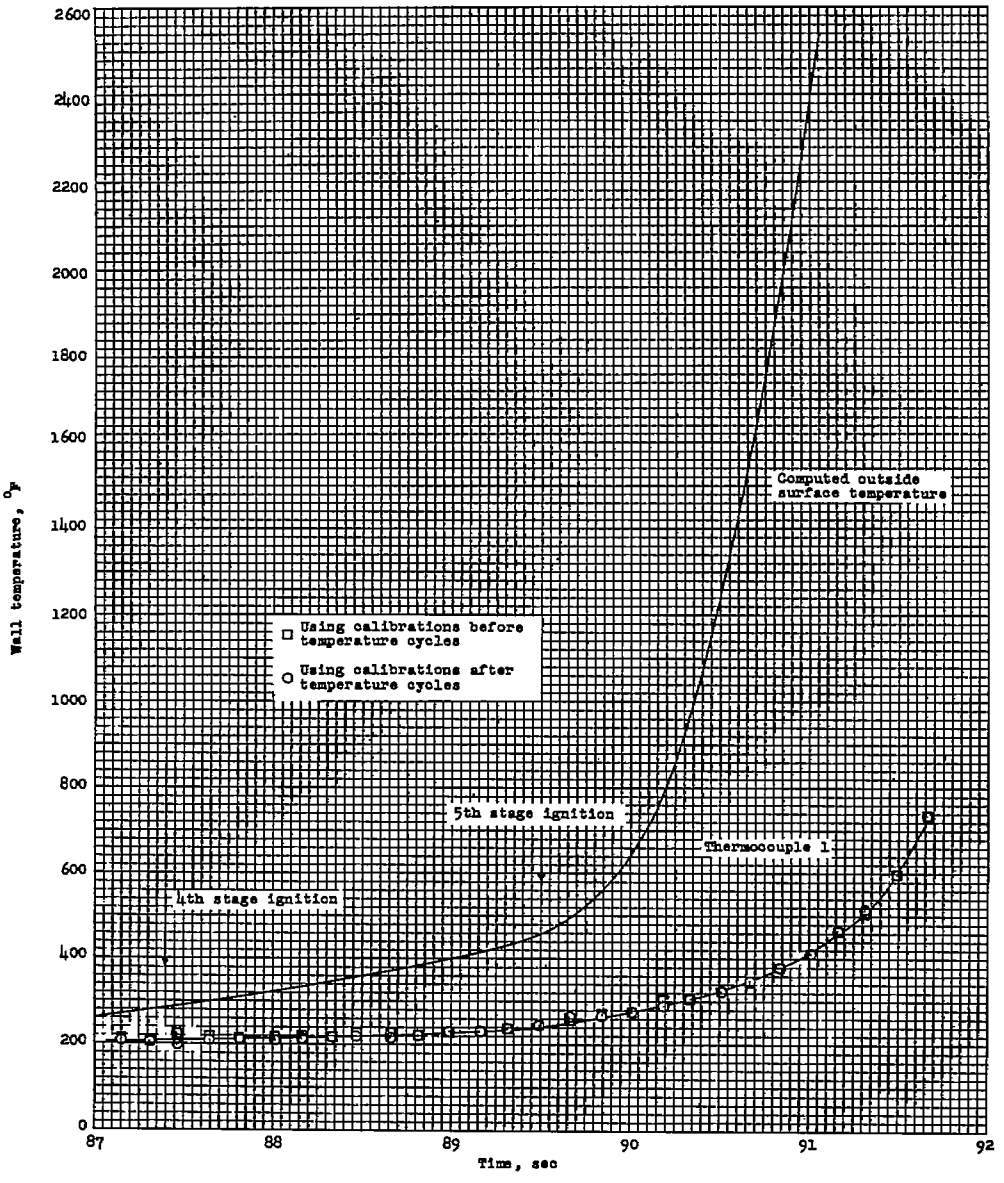

(c) Nose apex.

Figure 13.- Concluded.

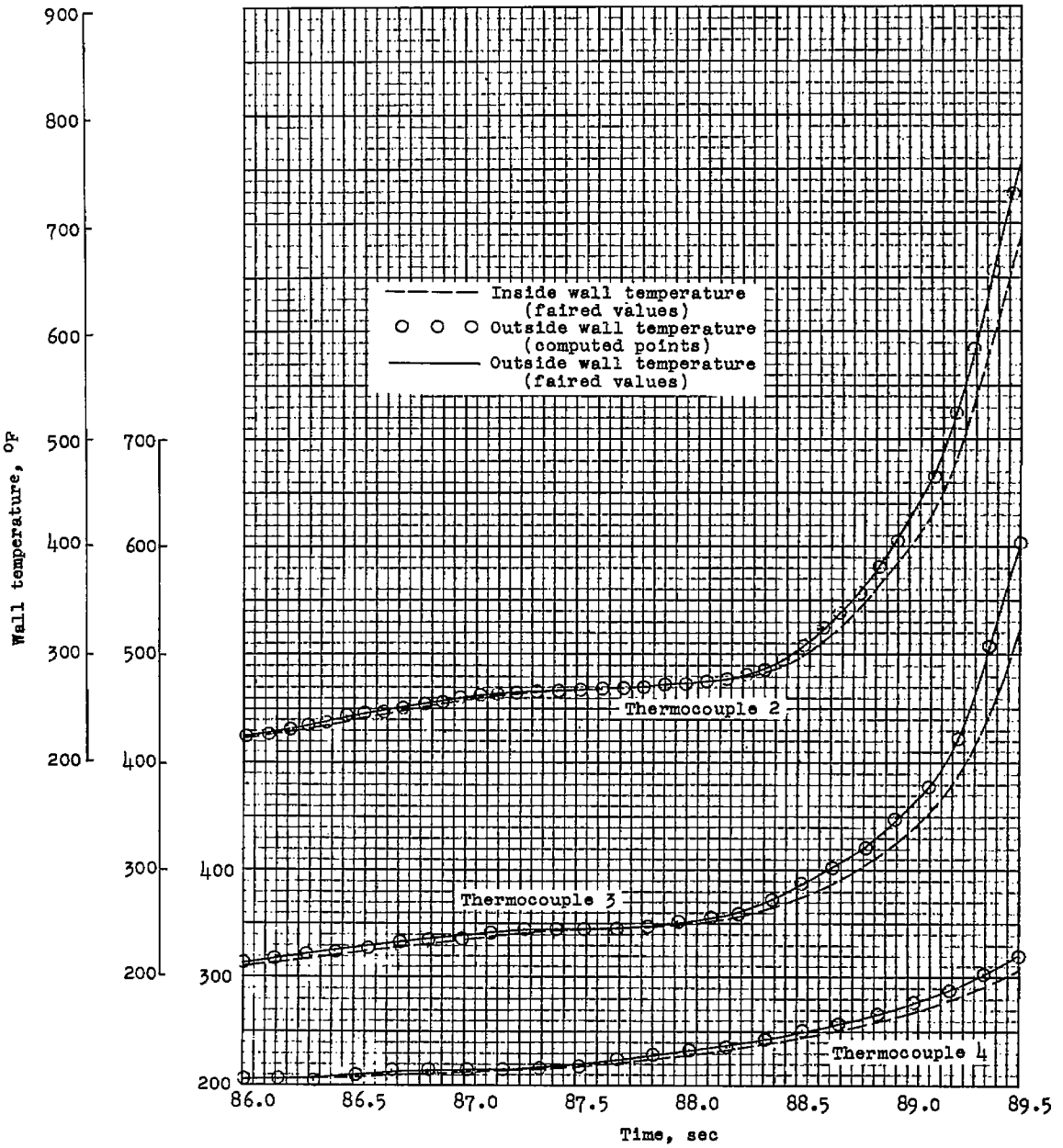

Figure 14.- Typical computed outside wall temperatures.

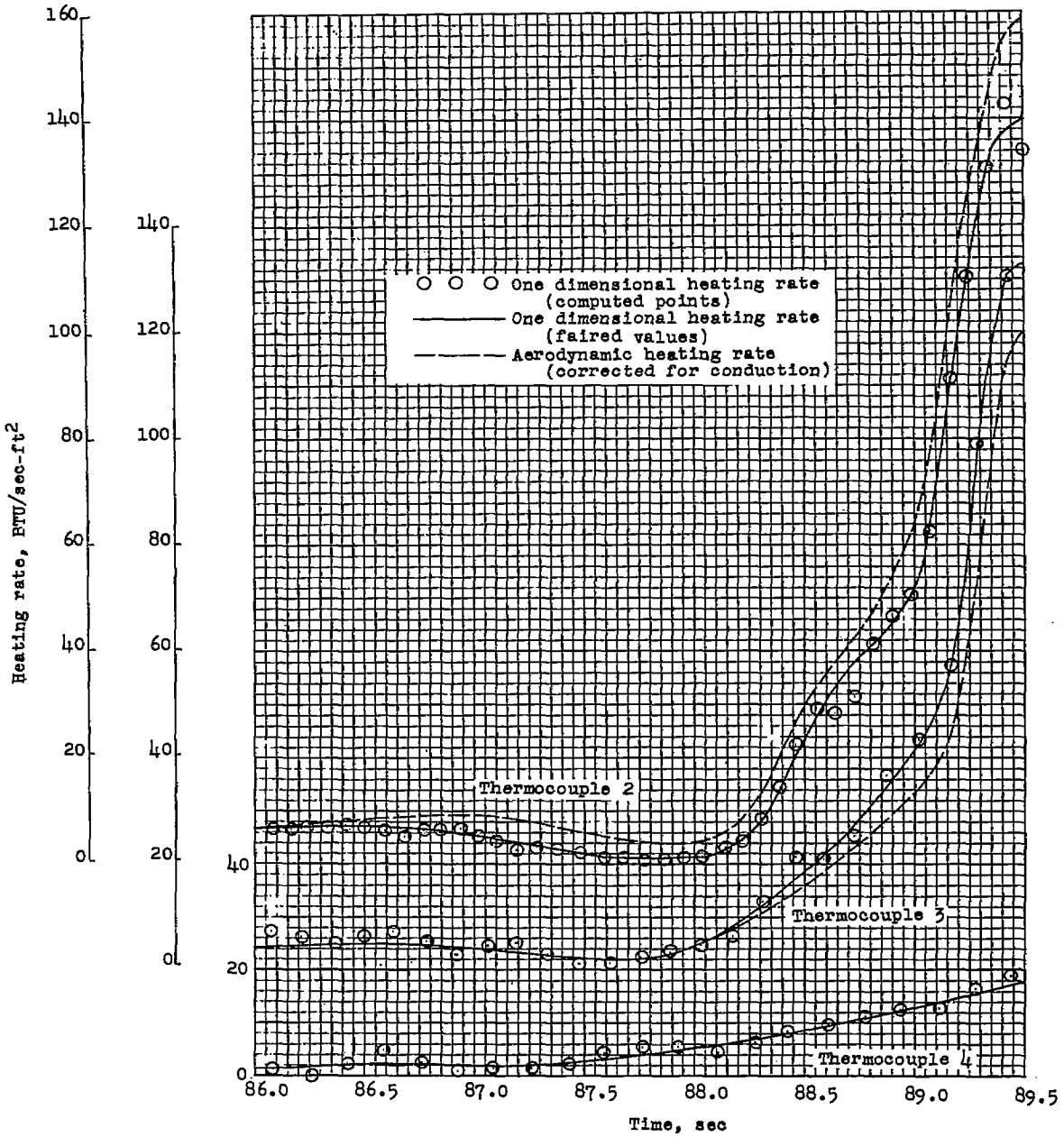

Figure 15.- Typical computed heating rates.

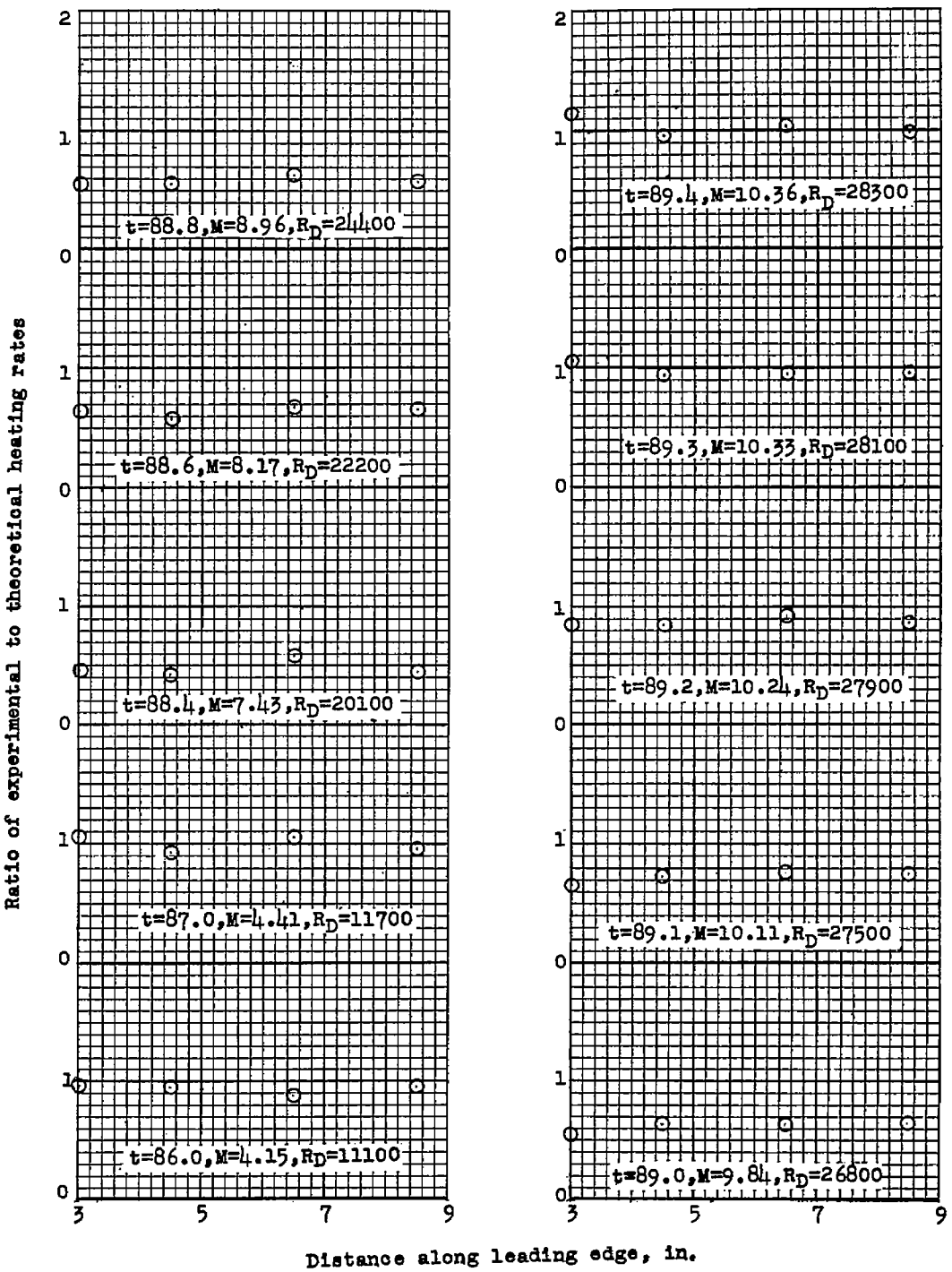

Figure 16.- Leading-edge heat-transfer data.

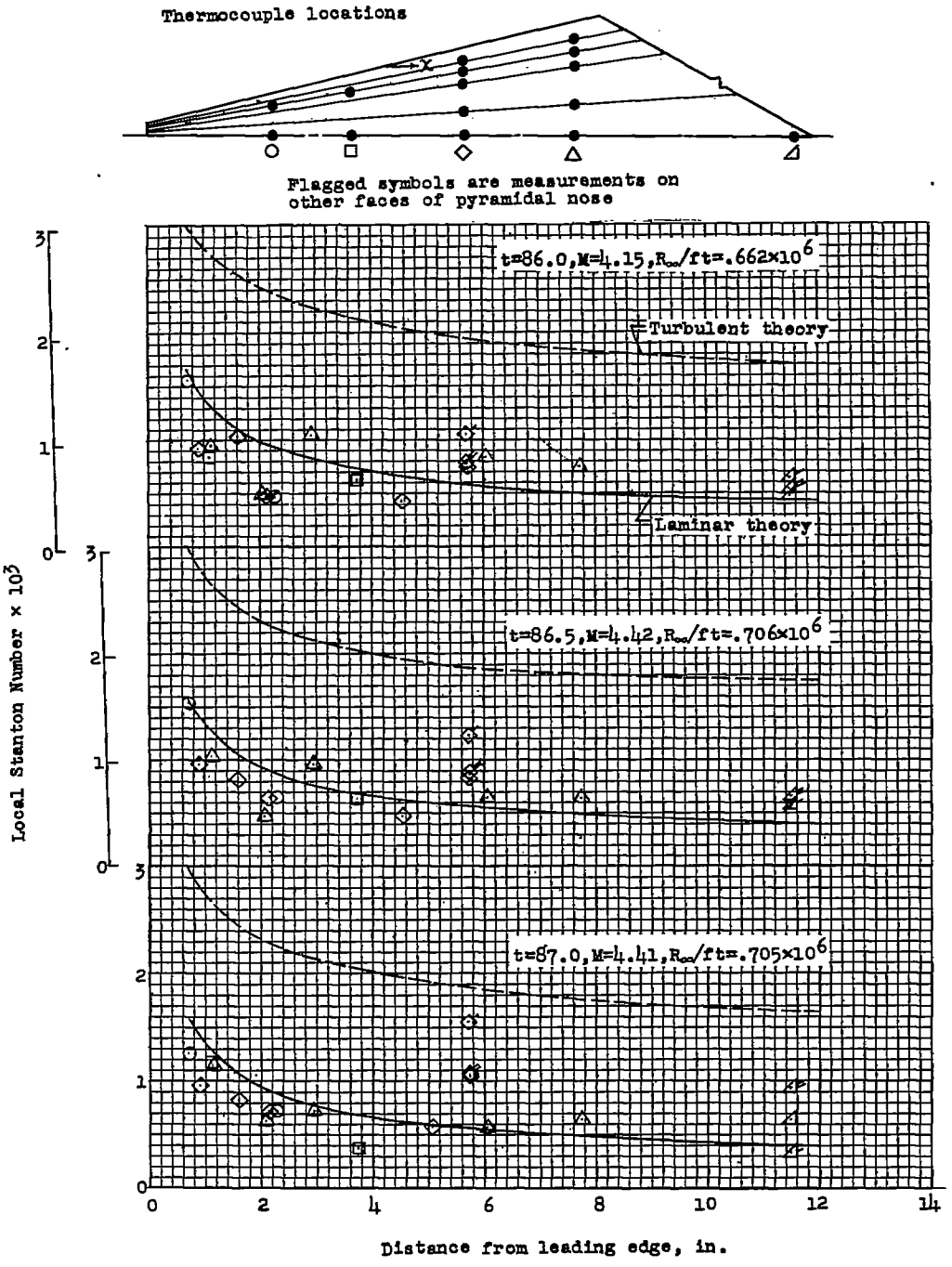

(a) Method 1; t = 86.0 to 87.0 seconds.

Figure 17.- Heat-transfer data for flat section of wing.

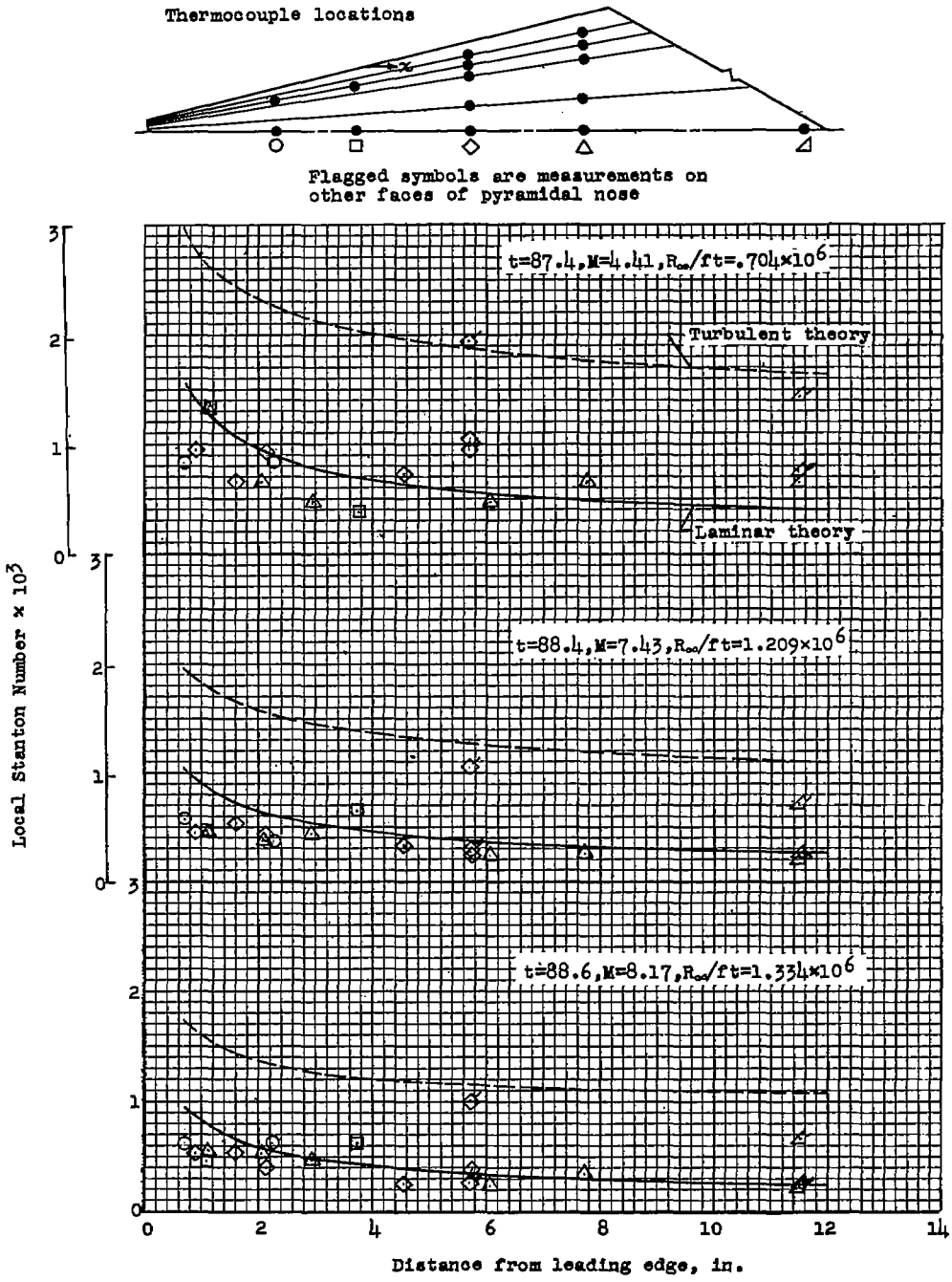

(b) Method 1; t = 87.4 to 88.6 seconds.

Figure 17.- Continued.

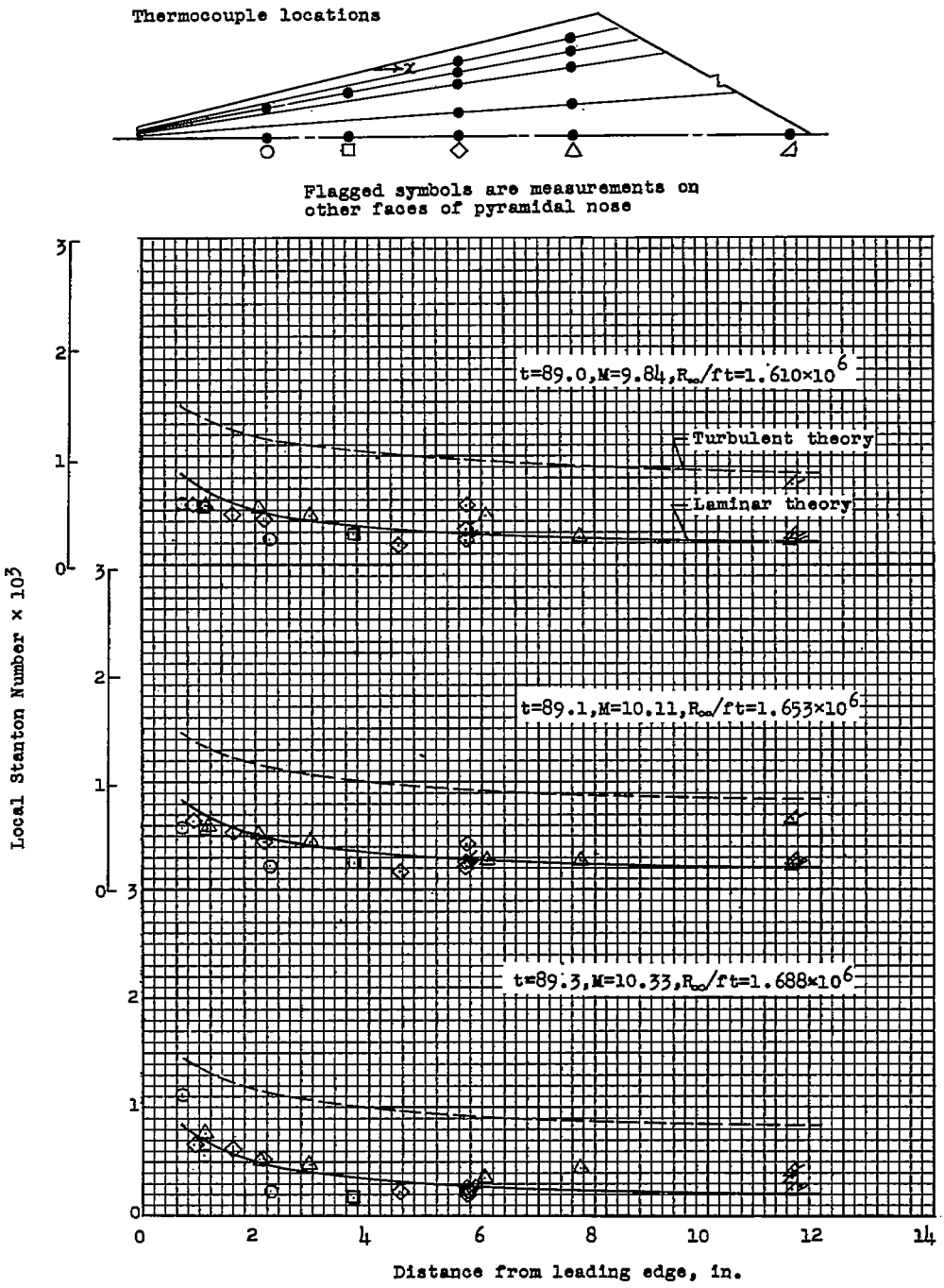

(c) Method 1; t = 89.0 to 89.3 seconds.

Figure 17.- Continued.

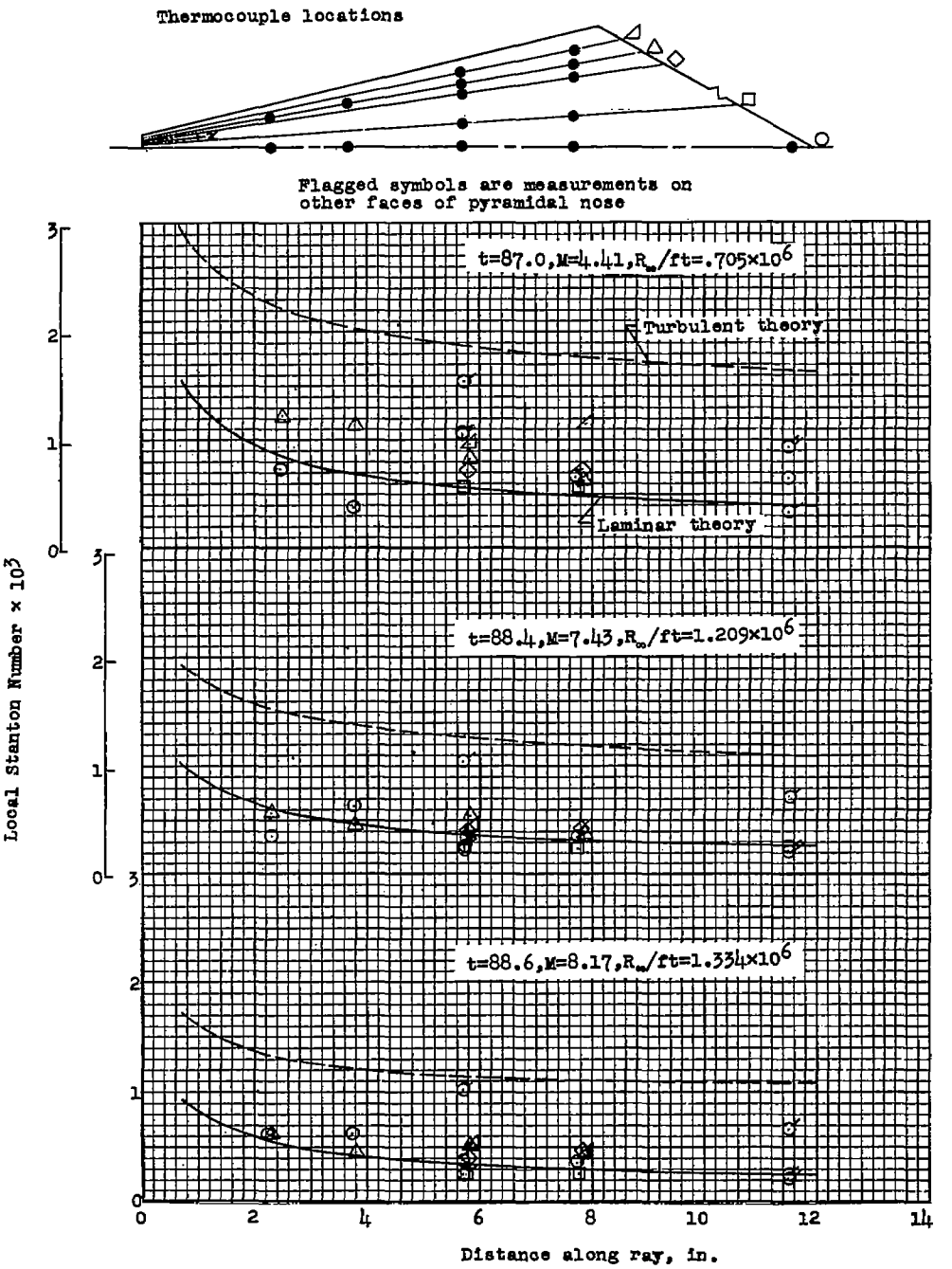

(d) Method 2; t = 87.0 to 88.6 seconds.

Figure 17.- Continued.

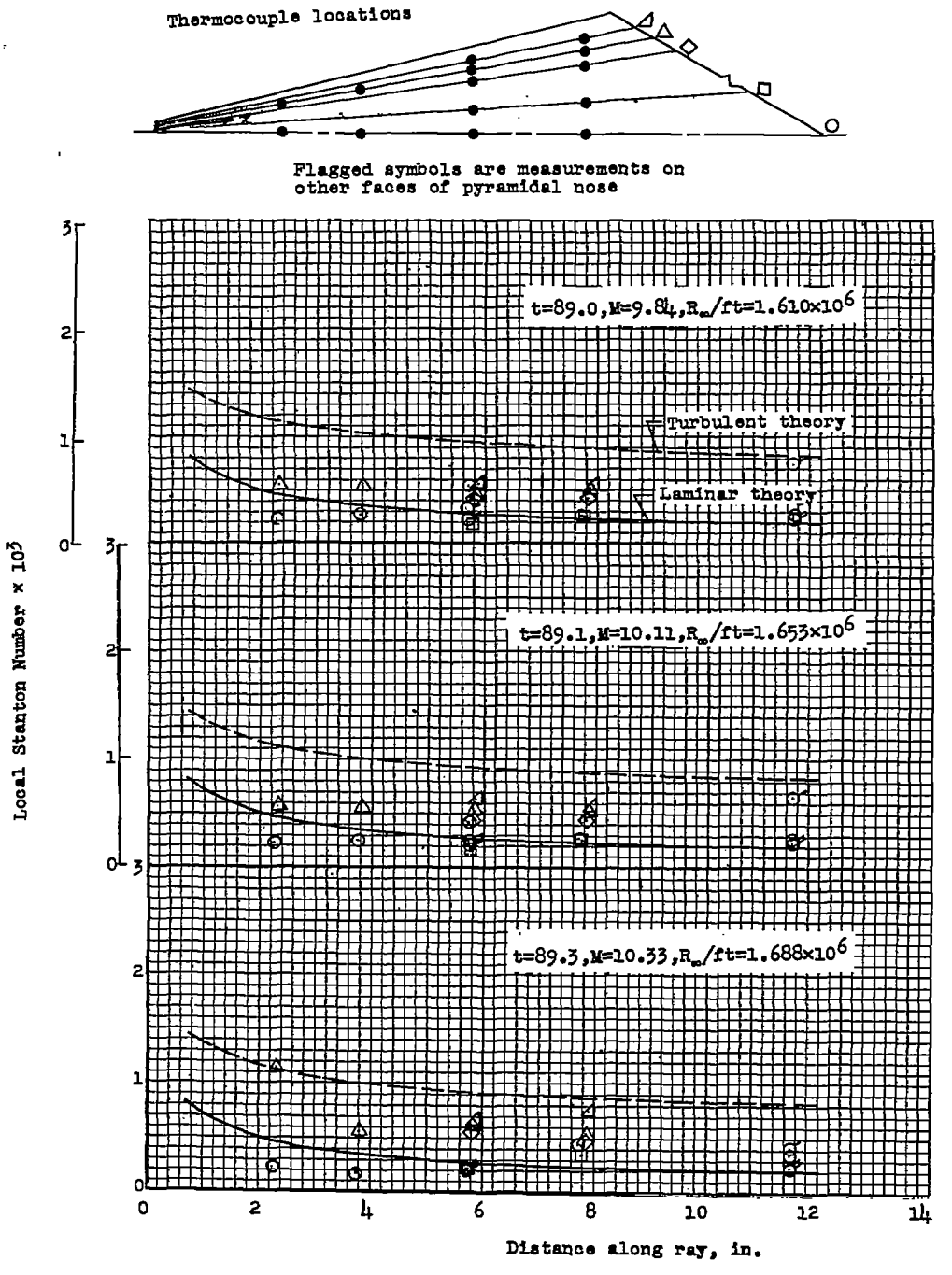

(e) Method 2; t = 89.0 to 89.3 seconds.

Figure 17.- Concluded.

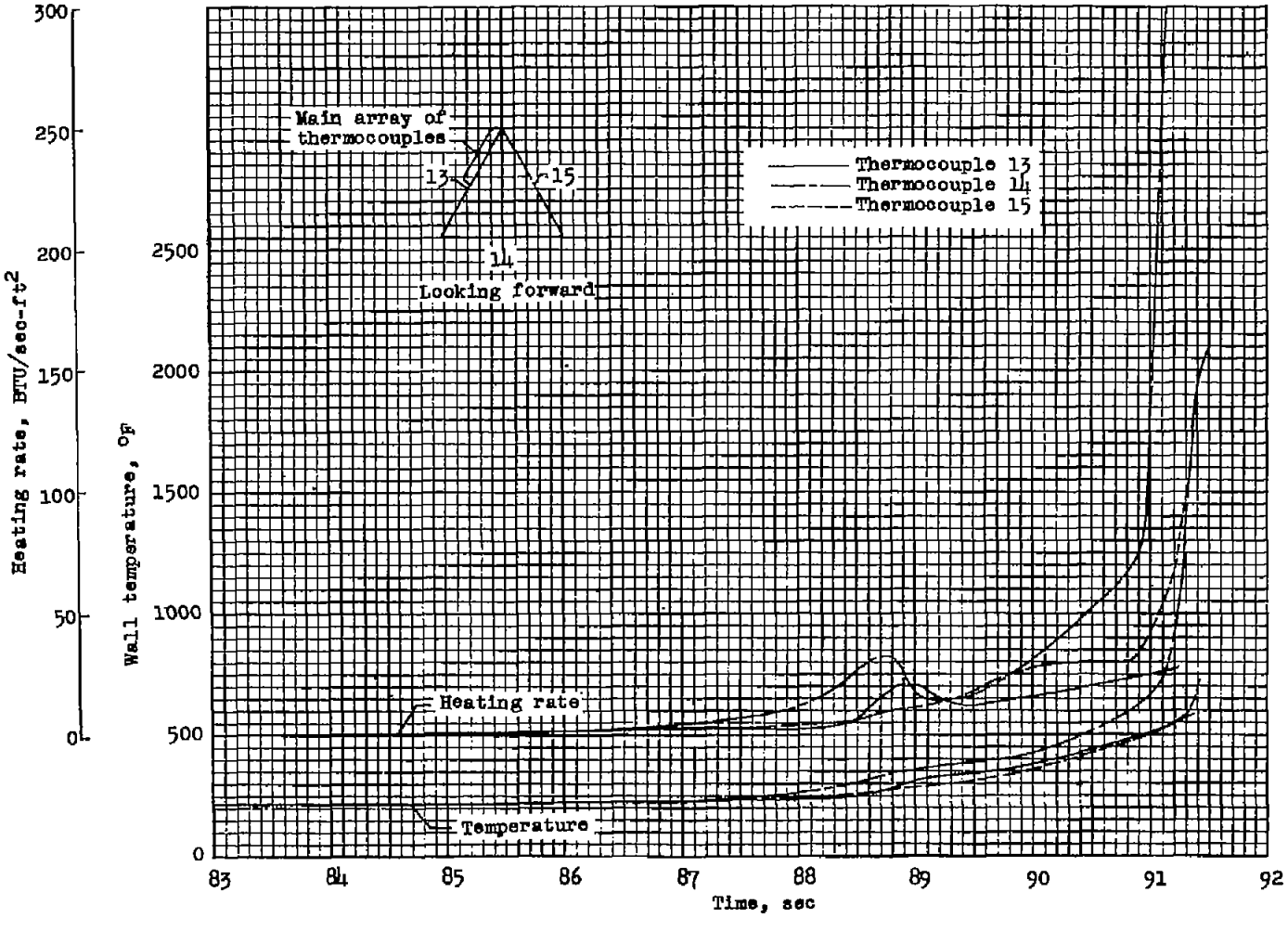

(a) Data at body station 6.5.

Figure 18.- Comparison of measurements on each of the three faces.

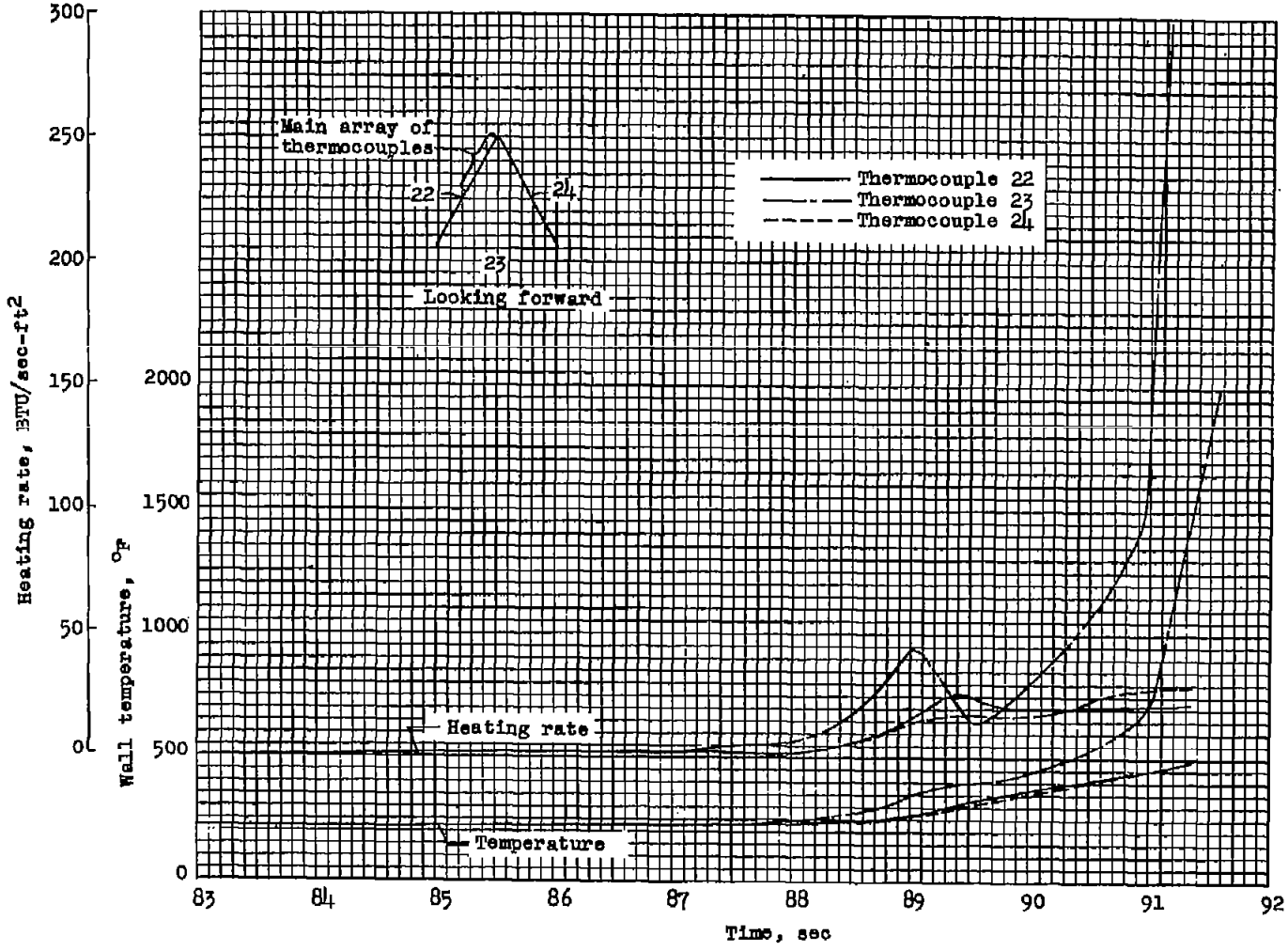

(b) Data at body station 12.5.

Figure 18.- Concluded.

NACA - Langley Field, Va.